AFRL-RV-PS-
TR-2014-0041

AFRL-RV-PS-
TR-2014-0041

SPACE WEATHER: MEASUREMENTS, MODELS AND PREDICTIONS

Patricia H. Doherty, et al.

Boston College
140 Commonwealth Avenue
Chestnut Hill, MA 02467

21 March 2014

Final Report

APPROVED FOR PUBLIC RELEASE; DISTRIBUTION IS UNLIMITED.

AIR FORCE RESEARCH LABORATORY
Space Vehicles Directorate
3550 Aberdeen Ave SE
AIR FORCE MATERIEL COMMAND
KIRTLAND AIR FORCE BASE, NM 87117-5776

DTIC COPY

NOTICE AND SIGNATURE PAGE

AFRL-RV-PS-TR-2014-0041 HAS BEEN REVIEWED AND IS APPROVED FOR PUBLICATION IN ACCORDANCE WITH ASSIGNED DISTRIBUTION STATEMENT.

//SIGNED//	//SIGNED//
Dr. Judy Fennelly Program Manager/RVBX	Edward J. Masterson, Colonel, USAF Chief, Battlespace Environment Division

REPORT DOCUMENTATION PAGE

Form Approved
OMB No. 0704-0188

1. REPORT DATE *(DD-MM-YYYY)*
21-03-2014

2. REPORT TYPE
Final Report

3. DATES COVERED *(From - To)*
11 Apr 2009 to 06 Jan 2014

4. TITLE AND SUBTITLE
Space Weather: Measurements, Models and Predictions

5a. CONTRACT NUMBER
FA8718-10-C-0001

5b. GRANT NUMBER

5c. PROGRAM ELEMENT NUMBER
61102F

6. AUTHOR(S)
Patricia H. Doherty, David Webb, Stuart Huston, Thomas Kuchar, Donald Mizuno, William Burke, Kara Perry, and James Sullivan

5d. PROJECT NUMBER
2301

5e. TASK NUMBER
PPM00009851

5f. WORK UNIT NUMBER
EF004615

7. PERFORMING ORGANIZATION NAME(S) AND ADDRESS(ES)

Boston College
140 Commonwealth Avenue
Chestnut Hill, MA 02467

8. PERFORMING ORGANIZATION REPORT NUMBER

9. SPONSORING / MONITORING AGENCY NAME(S) AND ADDRESS(ES)

Air Force Research Laboratory
Space Vehicles Directorate
3550 Aberdeen Avenue SE
Kirtland AFB, NM 87117-5776

10. SPONSOR/MONITOR'S ACRONYM(S)

AFRL/RVBX

11. SPONSOR/MONITOR'S REPORT NUMBER(S)
AFRL-RV-PS-TR-2014-0041

12. DISTRIBUTION / AVAILABILITY STATEMENT

Approved for public release; distribution is unlimited. (377ABW-2014-0456 dtd 16 Jun 2014)

13. SUPPLEMENTARY NOTES

14. ABSTRACT
Boston College has provided scientific and technical support to the Air Force Research Laboratory (AFRL) Space Vehicles Directorate to include a number of innovative research and analysis programs to understand the fundamental solar and magnetospheric processes and mechanisms that drive and control the Earth's space environment in order to understand, specify, anticipate, and mitigate the effects of space weather on Air Force systems.

15. SUBJECT TERMS
CME, Solar Flare, SWFL, Trapped Electron and Proton Model, AE-9/AP-9, TacSat4, AFGEOSpace, Langmuir Probe

16. SECURITY CLASSIFICATION OF:			17. LIMITATION OF ABSTRACT	18. NUMBER OF PAGES	19a. NAME OF RESPONSIBLE PERSON
					Dr. Judy Fennelly
a. REPORT	b. ABSTRACT	c. THIS PAGE			19b. TELEPHONE NUMBER
Unclassified	Unclassified	Unclassified	Unlimited	46	

Standard Form 298 (Rev. 8-98)
Prescribed by ANSI Std. Z39.18

This page is intentionally left blank.

Table of Contents

List of Figures

1. SUMMARY

The research performed under this contract was comprised of a number of innovative research and analysis programs to understand the fundamental solar and magnetospheric processes and mechanisms that drive and control the Earth's space environment in order to understand, specify, anticipate and mitigate the effects of space weather on Air Force systems. As part of our efforts, we supported this program with research and instrument development to study the origins and interplanetary (IP) propagation of disturbances that affect the geosphere and to support the mission and analyze the data from the AFRL Solar Mass Ejection Imager (SMEI) experiment, a heliospheric image/detector that observes and tracks coronal mass ejections from the Sun to Earth. This program includes support to AFRL to design and develop the next generation heliospheric imager system. Boston College also provides scientific and technical collaboration to AFRL/RVB to aid and enable the development and validation of the AE-9 and AP-9 models, the next-generation of trapped electron and proton models designed to replace the current AE-8 and AP-8 models and provide users with much-needed improvements in accuracy and additional capabilities. This work also addresses the development of enhanced versions of AFGEOSpace and the Heliospace analysis toolset. Finally, special projects in support of Earth's Space environmental studies are addressed throughout the duration of the contract. These include the analysis of various space sensors and satellite missions.

2. INTRODUCTION

This contract consisted of a number of projects in support of Space Weather: Measurements, Models and Predictions. In the following, we introduce each project, describe the analysis and provide the main results of our efforts.

3. METHODS, ASSUMPTIONS, AND PROCEDURES

3.1 Solar Origin and Interplanetary Propagation of Geoeffective Disturbances

One of the prime goals of this contract has been to understand the origins and interplanetary (IP) propagation of disturbances that affect the geosphere, and to develop, support and analyze the data from the Solar Mass Ejection Imager (SMEI) spacecraft experiment, designed to provide early warning and measurement of space hazards. The research studies have involved collecting and analyzing satellite and ground-based data sets of pertinent solar, IP and geomagnetic phenomena to address 3 general topics: (1) The solar eruptive phenomena which lead to sporadic geomagnetic storms; (2) IP shocks and other signatures of solar ejecta; and (3) The characteristics of IP disturbances which produce geomagnetic storms. The most important goal of the studies is to utilize data sets related to solar ejecta and their IP manifestations to define the origins and propagation characteristics of geoeffective disturbances. The work also involved the development and support of the SMEI spacecraft experiment and analysis of the data returned. SMEI was a proof-of-principle experiment for providing an early warning of 1-3 days of the arrival at Earth of a coronal mass ejection (CME), and measurements of crucial geoeffective parameters of the CME.

3.1.1 Coronal Mass Ejections (CMEs)

Coronal mass ejections consist of large structures containing plasma and magnetic fields that are expelled from the Sun into the heliosphere. They are of interest for both scientific and technological reasons; scientifically because they are responsible for the removal of built-up magnetic energy and plasma from the solar corona, and because technologically they are responsible for the most extreme Space Weather effects at Earth, as well as at other planets and spacecraft throughout the heliosphere. The CME plasma is entrained on expanding magnetic fields, which commonly have the form of helical field lines with changing pitch angles, i.e., a flux rope.

The recent solar minimum (2008-2009) between solar cycles 23 and 24 was unusually prolonged, with record numbers of sunspot-free days, record low solar polar magnetic fields, and record high levels of cosmic ray flux. There were broad-ranging terrestrial responses to this inactivity of the Sun. BC was involved in the international Whole Heliosphere Interval (WHI) program to study this minimum period and compare it with previous minima [1, 2, 3, 4]. Most of the ~60 coronal mass ejections (CMEs) during WHI occurred during the first, active half of the interval. The origins and early development of the CMEs and their associated active regions were analyzed [5]. The overall evolution of the active regions and CMEs were analyzed in the context of the three rotations centered on CR 2068.

The STEREO Heliospheric Imagers (HIs) are part of the SECCHI suite of imaging telescopes on each spacecraft and view the inner heliosphere starting at an elongation of 4° from the Sun. The HI telescopes observe up to a 90° range in position angle, centered on the ecliptic and viewing either east (HI-A) or west (HI-B) of the Sun-Earth line. Combined with the SECCHI coronagraphs, the HIs provide a continuous view from the Sun to elongations of ~90° from the Sun-STEREO line. During the overlapping period of their missions, 2007 through 2011, SMEI provided global context observations for the SECCHI HIs as well as a "third-eye" view from Earth orbit. The combination of the limited-field HI and all-sky SMEI observations form a unique data set that have already provided fundamentally new insights into CMEs. The BC group and collaborators were involved in many new studies using both SMEI and SECCHI data that are helping develop a deeper understanding of the structure of CMEs and how they propagate in the heliosphere [6]. Results using 3D global density reconstructions of the propagation of CMEs with SMEI and/or SECCHI HI data were published by [7, 8, 9, 10, 11, 12, 13, 14, 15].

Although we know the importance of CMEs in the evolution and propagation of geoeffective disturbances, their solar origins remain obscure. CMEs often exhibit a "three-part" structure consisting of a bright leading arc followed by a darker, low-density cavity and bright core of denser material. With the 3-D views from SOHO and STEREO it is now clear that most CMEs contain flux ropes and are likely associated with "magnetic clouds" detected in-situ by spacecraft. The frequency of occurrence of CMEs tends to track the solar sunspot cycle in both phase and amplitude, but during the recent cycle 24 this relationship is diverging and is an area we are studying. Solar surface activity associated with CMEs includes the formation of dimming regions, long-lived loop arcades, flaring active regions, large-scale coronal waves, and filament eruptions and in the corona with large-scale, closed structures such as coronal streamers. During this period we have studied all these structures, and currently are investigating flares, dimming regions and arcades using SDO EVE spectral and AIA imaging observations [16]. These data have great potential for space weather forecasting.

The trailing structures of CMEs provide important information on magnetic field line reconnection and kinematics of CMEs. The SOHO LASCO coronagraphs have revealed concave-outward, flux rope-like structures in nearly half of all CMEs, and trailing ray-like features suggestive of current sheets created during reconnection. BC personnel have been at the forefront of eruptive current sheet studies, were part of the ISSI Workshop on Eruptive Current Sheets [17], and have compiled a catalog of LASCO post-CME current sheets/rays and are analyzing them [18, 19].

3.1.2 Solar Flares

A study was performed involving the thermal evolution of solar flares using data from the Extreme ultraviolet Variability Experiment (EVE) on the recently launched NASA Solar Dynamics Observatory (SDO). EVE has the highest spectral and temporal coverage of any EUV experiment designed to study space weather effects. About 20 flares observed over a 4-month period are being studied. Their hot coronal emissions (~3 MK) often have large secondary peaks that appear many minutes to hours after an eruptive compact flare event. In contrast, the cool coronal emissions (~0.5 - 1.5 MK) usually dim immediately after the flare onset and do not recover until after the delayed second peak. We refer to this period of 1-5 hours after the main flare phase as the late phase. Our analysis of these flare events suggests that the late phase involves hot coronal loops near the flaring region, but not directly related to the original flaring loop system [16].

3.1.3 The Solar Energetic Particle Model (SEPMOD)

We initiated a study on Forecasting Arrival Times of Shock-Driven Solar Energetic Particles. The objective of this study was to test and validate the numerical SEPMOD model, which estimates the solar energetic particle (SEP) intensity profiles for 10 MeV to 100 MeV energies at Earth. SEPMOD can be used with a heliospheric solar wind model, such as Wang-Sheeley-Arge (WSA)-Enlil, together with the geometric “cone” description of a CME. This modeling objective supports the AFRL/RVBXS effort of forecasting the arrival times of CME shock-driven SEPs in order to mitigate their potentially harmful effects on Air Force satellites.

Dr. Janet Luhmann was consulted in-depth with about her SEPMOD code. The current version of this model uses output files generated by the Wang-Sheeley-Arge (WSA)-Enlil-cone modeling system. Dr. Luhmann gave training sessions from how to use her SEPMOD model and how to process the output files. At the conclusion of this meeting she shared her numerical code and the supporting code documentation. The SEPMOD code has been installed and are tested the using a number of test case files provided by Dr. Luhmann. In order to rigorously test the model with newer retrospective SEP events, the model developer’s numerical version of the WSA-Enlil heliospheric solar wind model that produces output files required by SEPMOD was used. Using the current state-of-knowledge of CME-shock driven solar energetic particles, a compilation was created of recent SEP events observed at earth.

3.1.4 Solar Mass Ejection Imager (SMEI)

CMEs have been observed in white light for decades with coronagraphs viewing near the Sun that observe Thomson-scattered brightness of sunlight scattered from heliospheric electrons. Over the last decade heliospheric imagers, also viewing in white light, were developed and launched. The Solar Mass Ejection Imager (SMEI), initially funded by NASA and AFRL, was launched on the Coriolis STP mission in January 2003 and consisted of three baffled cameras whose 3° x 60° fields of view were aligned in their long dimension to achieve a combined ~160°-wide field of view that scanned most of the sky every 102-minute orbit. The majority of SMEI data have an angular resolution of ~0.2°. Its global sky coverage permitted continuous imaging sequences and, thus, a view of heliospheric structures as they moved across the sky over a wide range of solar elongations. This type of analysis of SMEI data has provided a unique new perspective on heliospheric observations of solar disturbances (e.g., [20]).

Modeling the propagation of CMEs necessarily entails validation with heliospheric imaging. However, the Thompson scattered light from CMEs is several orders of magnitude fainter than the backgrounds they traverse through the heliosphere, so careful processing is needed of the images to remove the backgrounds but leave the CME emission. BC has a legacy of working with heliospheric imaging as well as CME tracking and modeling. AFRL and BC were responsible for the data pipeline and image construction of the SMEI Project, and producing “quick-look” maps for near-real time (NRT) space weather forecasting. The University of California at San Diego (UCSD) SMEI pipeline was designed to maintain as much as possible of the original SMEI data frame resolution and photometric precision. BC has worked closely with the UCSD SMEI group in processing and analysis of SMEI data on CMEs [10, 11, 12, 7].

The AFRL/BC group produced Flexible Image Transport (FITS) images in Aitoff and fisheye projections for NRT forecasting with 1° spatial resolution, and higher resolution maps for archiving purposes. The UCSD database now includes over 4 terabytes (TB) of individual data frame images, and over 6 TB of data products available at: http://smei.ucsd.edu/. The BC team has used a set of archived difference images to identify and track CMEs in the SMEI data, and these CMEs have been cataloged using an AFRL/BC processing technique. Over the 8.5 year lifetime of the mission, we have identified >400 events using this technique.

At BC many analyses of SMEI CME data was preformed, especially for individual events and on the solar-cycle variation of CME rates. In addition, the backgrounds in SMEI images provide a wealth of useful astronomical data which was exploited by the BC group. Such studies have included the detection of high altitude aurorae [21], the disruption of comet tails [22], analysis and modeling of the zodiacal dust, and the long-term monitoring of bright stars [23]. The zodiacal dust appears as scattered sunlight but it has mostly been observed in the infrared with visible-light models lacking. The SMEI data provide unique data to study and model the zodiacal light since SMEI continually observed it for nearly 8½ years and a realistic 3-D model of dust cloud is possible. The SMEI database also provides long-term monitoring of bright stars. Many of these stars are used as calibrators for astronomical surveys, yet their long term stability as such has rarely been investigated. The AFRL network of calibration stars uses many of these bright stars as references in the infrared. This is now being extended into the visible and the SMEI database is being used to determine any variability in the visible. Finally, SMEI made many serendipitous observations of satellites and space debris that crossed the field of view of the cameras. Some studies of the nature and origin of this debris has been made by the BC group, most recently of the origin of a debris swarm that was seen near the cameras [24].

As solar activity increased, SMEI began to observe more intense CMEs/storms as they traversed the heliosphere. These observations were measured and identified and movies of SMEI images with the IDs were generated in each case. Also, with more accurate timing and positions, archived SMEI data were examined for launches that were not observed in the SMEI final processed images. In these instances, the individual frame data were examined in the eventuality that the processing pipeline for the SMEI imaging removed evidence of the launches as an artifact. For the first few cases, one additional launch was observed. A catalog of such “missed” launches has been compiled.

A SMEI measuring tool was created to provide measurements of CMEs/storms as they traversed the heliosphere. Minor updates were incorporated into the software over the lifetime of the mission. Also the software was modified to provide a more user-friendly GUI for operators at the Space Weather Forecast Laboratory (SWFL). It provided the user with an estimate of the launch time for the measured solar disturbance. Though these were calculated in the original program, the results are provided to the user as a summary. Re-evaluation of the state of the health and responsivity of the cameras over the mission lifetime was made continually during the mission. Software was written to extract the photometry of individual stars on each frame of data by fitting each star with an interpolated point response function (PRF). A catalog of the 5800 brightest stars (down to 6th magnitude) was used to locate the stars on individual frames. All the current pipeline corrections used for imaging were applied to each frame (dark correction, flat field, spike removal, optical path correction, etc).

During this period we continued to maintain and update the SMEI catalog of CMEs and the SMEI publications list. A summary of the mission goals and lessons learned was also contributed to by BC researchers. After the termination of the SMEI mission in 2011, a comprehensive paper describing its scientific discoveries and legacy was published [25].

3.1.5 Space Weather Forecast Lab (SWFL)

BC team members were also an integral part of AFRL’s Space Weather Forecast Laboratory (SWFL). SWFL was created in 2007 to integrate research advances in several disciplines to provide new or improved end-user capability to specify and forecast:

1) satellite anomaly hazards
2) impacts of the ionosphere’s state and solar emissions on radio wave propagation, interference and scintillation
3) upper atmospheric changes that affect satellite drag.

BC team members attended routine meetings of SWFL, led work groups and contributed to research and discussion in support of SWFL.

One was using only White Light (Heliospheric Imager) data for forecasting. The goal was to demonstrate and evaluate the use of SMEI data to directly estimate CME propagation speed and to forecast shock and CME arrival times at Earth. At the time of the AFRL-East move validation was in progress comparing predicted arrival times with L1/ACE indicators and with heliospheric imagery to assess accuracy of arrival time estimates. Part of this effort was to validate the Tappin-Howard propagation model developed with AFRL resources. The Tappin-Howard model assimilates heliospheric image data, such as from SMEI or the STEREO HI imagers, to track and forecast CME arrivals. The model was used in several studies for validation for space weather forecasting [26, 27]. We also developed a tracking tool for testing for operational use at AFWA. Both the tracking tool and the Tappen-Howard (T-H) model were evaluated from 2010-2011 using SMEI data to predict the speed and time of arrival (ToA) of CMEs at 1 AU vs the time that the forecast was actually made [28]. We were also involved in improving predictions of CME/shock arrival times at Earth using the HAF-v2 solar wind model and resulting storm strength. Another SWFL task was to evaluate the performance of several models, such as WSA-Enlil and HAF that forecast solar wind and IMF characteristics for a representative period of a solar cycle.

BC personnel were also involved in intercomparisons of forecasts of space weather events, using LASCO, STEREO and other datasets. During 2010–2011, STEREO Group members made near-real time event predictions for three events: 8–12 April 2010, the 30 July–4 August 2010 series of multiple events, and the 15–18 February 2011 X–class flare–CME [29, 30]. The Group predictions for these three sets of events were based on several models and techniques, including geometric localization and polarization, HI “J–plots”, a NOAA empirical model, the HAFv2 model, the WSA+Enlil model, the Shock Time of Arrival (STOA) model, the Empirical Shock Arrival model, and the Tappin-Howard model. For all three event periods, the prediction accuracy averaged 8.0 hr. with a large range, an improvement over the typical time–of–arrival uncertainties in the past literature of 11–12 hours. The lead or warning time averaged ∼1 day. These results showed that use of heliospheric imaging data improves forecast performance, and that a mission with imagers dedicated to space weather will provide the best performance.

3.1.6. Hybrid Space Weather Forecasting and Modeling

BC collaborated to support AFRL’s efforts in developing a Next Generation Heliospheric Imager, assisting Janet Johnston of AFRL and world-wide experts in two workshops held at Sacramento Peak Observatory, NM on developing missions such as to the Sun-Earth L5 Lagrangian point. Such missions would involve both heliophysics and space weather research and forecasting, with an array of instruments including a Next Generation Heliospheric Imager [31, 32].

The development of hybrid space weather forecasting methods was performed under this effort. Several categories were developed based on precursor and advance warning time frame (e.g. forecast to nowcast to post-cast). These time frames can range from days to hours. Various satellites/observations were tagged as being the most relevant for these forecast regimes. The types of observations/ precursors (.e.g. coronal holes, filament eruptions, sigmoids) and the probabilities of an event with each of these categories were refined.

As part of the hybrid forecasting method, a CME prediction algorithm was developed based on climatology data from the previous solar cycle. This is based both on sunspot number and CME counts from Cycle 23. The two data sets are adjusted and scaled for the current cycle, since solar activity is at a reduced rate compared to the previous solar cycle. Probabilities are calculated for the occurrence of CMEs on any given day in the solar cycle as well as the trends of CME occurrence within the cycle. Recurrence and persistence probabilities of these events which will give forecasters near-term probabilities as well as historical ones were investigated. The output of one predictor is the monthly averaged CME rate in CMEs/day. Further adjustments are required since the last solar cycle, minimum to minimum, indicated a 12.5 year cycle, rather than the canonical 11 years.

Since BC contributed the current and persistence CME rate for 2010 to the weekly SWFL forecast meeting, we folded these statistics into the above prediction algorithm for a more accurate shift/scaling of the previous cycle's numbers. There is a known bias in the previous cycle's count onward from about 2005. Our goal was to correct this bias in our prediction algorithm

Also, as part of the hybrid method, we looked at the persistence CME rates from east-to-west limb events. That is, determining the number of events on any given date and determining the number of events on the opposite limb one-half a solar rotation (+/- one day) later. This will give an indication of persistent solar activity. Currently the CDAW catalog data does not give the surface source regions for these events, so a proxy of position angle in the catalog is being used to indicate limb location in lieu of the actual solar surface coordinates. For this proxy, it was determined that events with position angles within 20 degrees of solar equator during a period of solar minimum activity reduce confusion. Early results showed a 20% persistence rate from limb-to-limb.

3.2 Space Particle Modeling: The Next Generation Trapped Electron and Proton Models

The radiation belts and plasma in the Earth's magnetosphere pose hazards to satellite systems that restrict design and orbit options with a resultant impact on mission performance and cost. For decades, the standard space environment specification used by the engineering community was provided by the NASA AE-8 and AP-8 trapped radiation belt models. With well known limitations on their validity, AFRL/RVBX initiated collaboration with the National Reconnaissance Office (NRO), Aerospace Corporation and Los Alamos National Laboratory (LANL) to develop the next generation trapped electron and proton models, to be designated AE-9 and AP-9. These models will replace the AE-8 and AP-8 models and provide users with much-needed improvements in accuracy and additional capabilities not possible with the current models.

During the course of this contract, Boston College provided scientific and technical support to AFRL/RVBX to enable the development and validation of AE-9 and AP-9 models. BC activities in the project involved processing data from sensors on multiple spacecraft and organizing it into a model suitable for spacecraft design. The primary objectives of the effort were to 1) Improve the overall accuracy of the models; 2) Provide indicators of the uncertainty in the model due to natural variability and instrument uncertainty; 3) Cover a broad energy range including hot plasma, relativistic electrons and highly energetic protons; and 4) Provide complete spatial coverage.

The following covers the prime activities provided by BC team members for this effort. BC staff member, Stuart Huston, was instrumental in this project.

3.2.1 Proton Flux Maps. Our support activities began with the development of procedures for binning the proton fluxes obtained from spectral inversion of detectors on several spacecraft into the standard grid established for the AP-9 model. This also involved developing techniques for converting from one coordinate system (e.g., the invariant coordinate system used for the model) to another (e.g., the latitude-radius system which is a more intuitive mapping in physical space).

The binning/mapping exercise above revealed that the coordinate system based on adiabatic invariants results in major inaccuracies at low altitudes. The inaccuracy is due to the fact that the trapped particle flux is controlled more by the atmospheric density than by the magnetic field, and the adiabatic invariance is violated. Several new systems were investigated, based on the altitude that a particle reaches as it drifts around the Earth. Data from several spacecraft have been organized in several ways in order to determine which systems work the best. Several possible coordinates have shown great promise in providing much improved model accuracy at low altitudes, as well as providing accurate temporal variations due to the solar cycle and the changing geomagnetic field.

The results of this work were included in a briefing on proton flux mapping that was presented at the Critical Design Review for AE9/AP9 held at the Aerospace Corporation in November 2009.

3.2.2 Data Sources, Processing and Analysis. Key data for the new models include data recorded by instruments on the TSX5, S3-3, Polar, Azur and TacSat4 spacecraft. Boston College has supported the acquisition, processing and analysis of these satellite sensor data for developing the radiation belt models, AE-9 and AP-9

One of our data processing objectives was to generate and maintain the Compact Environmental Anomaly Sensor Experiment (CEASE) science and ephemeris databases. CEASE consists of a small environmental hazard detection system, which is both lightweight and has low power requirements. The total package provides data on radiation dose, single event upsets, and charging. A software system has been developed that will take the prime data set, the CEASE Science file, and parse the data into individual time tagged data base files. CEASE data provided throughout the duration of this project was processed and provided to AFRL.

Initial tasks also involved preparing data for our use. This included cleaning the data to reveal and remove potential contamination (e.g., counts from electrons in a channel that is supposed to be measuring protons), dead-time issues, and other problems that might make the data less useful. Data cleaning was performed for the TSX5/CEASE data set; this process revealed no significant problems. Figure 1 shows an example of plotting counts from a proton channel (D05 on the y-axis) against counts in a channel that measures both electrons and protons (D01 on the x-axis). The plot reveals that D05 is responding to electrons in the outer zone, but simple filters can eliminate data from the region where the contamination occurs.

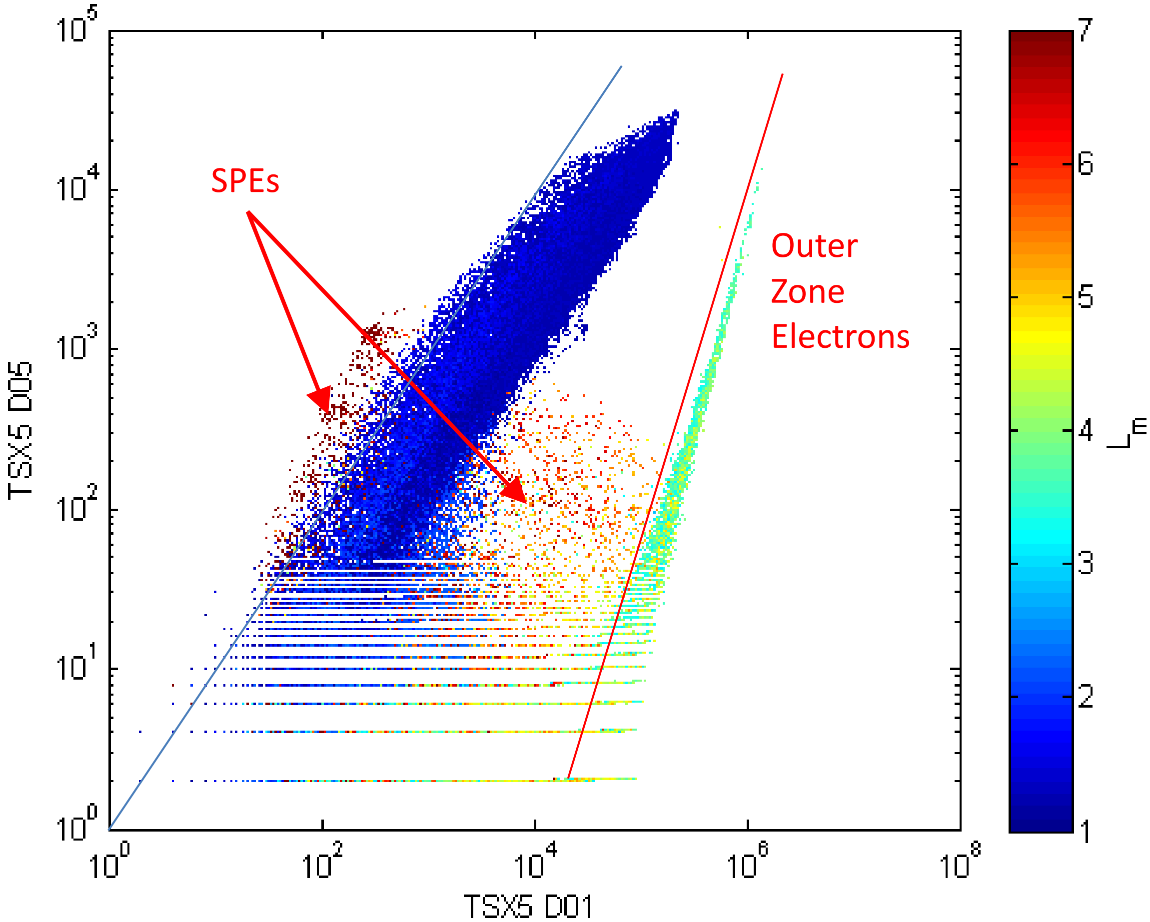

Figure 1. Example of cross-plotting counts in two different channels to reveal potential contamination.

Processing of S3-3 Proton Data

The S3-3 satellite operated from 1976 through 1979 and contained a proton telescope which measured protons from 80 to 3000 keV energy. This energy range is very important for phenomena such as surface dose on spacecraft, but is very difficult to measure. The S3-3 data set is nearly unique for this energy range and coverage of the inner zone.

Processing included:

- Writing MATLAB routines to read the binary data files and merge them with adiabatic invariant data calculated by AFRL.
- Performing "data cleaning" to identify potential sources of contamination, remove noise from the data, and identify any other issues.
- Calculate spectral correction factors. The S3-3 proton telescope has broad energy channels, and the effective geometric factor of each channel depends on the shape of

the flux spectrum within that channel. A method was developed to determine a correction factor by assuming a power-law spectrum within the channel; the power-law exponent was estimated using measured fluxes in adjacent channels. This correction was applied to the measured fluxes.

- Mapping fluxes in adiabatic invariant coordinates. Figure 2 contains an example of these maps.

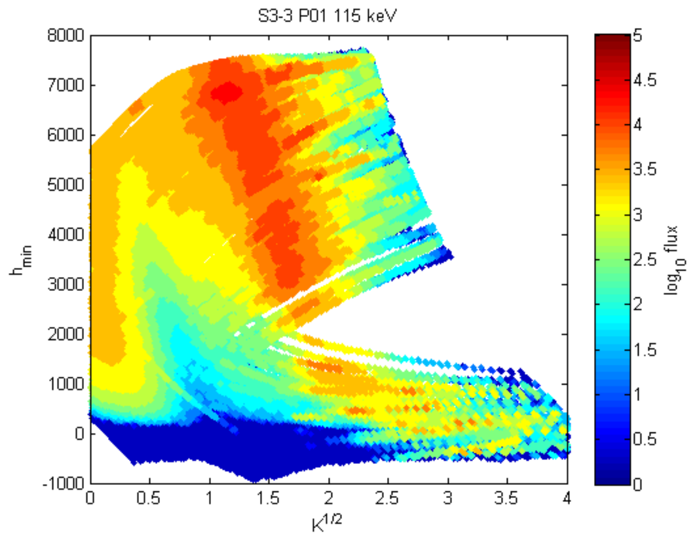

Figure 2. Fluxes from the S3-3 proton telescope mapped in adiabatic invariant coordinates.

Processing S3-3 Electron Data

Electron data from S3-3 was processed in the same way as the proton data. One of the significant aspects of this processing was the "self-calibration" of the S3-3 Magnetic Electron Spectrometer, which was needed in order to develop estimates of the uncertainty of the measurements. For many instruments used in this project, similar measurements are available for different sensors in the same region of space at the same time; these are referred to as conjunctions. When conjunctions are available, it is possible to cross-calibrate the different detectors and obtain error estimates. For S3-3, no comparable instruments were available for conjunctions, and so a "self-conjunction" approach was taken. Successive passes through bins with a time difference of less than one day were treated as conjunctions, and the flux from one pass was compared to the flux during another pass. The standard deviation of the difference in log(flux) between successive passes was taken as the error estimate for each energy channel of the detector. One problem arose because the higher energies exhibited a bi-modal distribution, with a high energy tail present in some spectra and absent in others. Only spectra with the high energy tail were used for the self-calibration analysis. However, future analysis of the data could reveal interesting physics about the presence or absence of the tail. Figure 3 illustrates the self-calibration analysis.

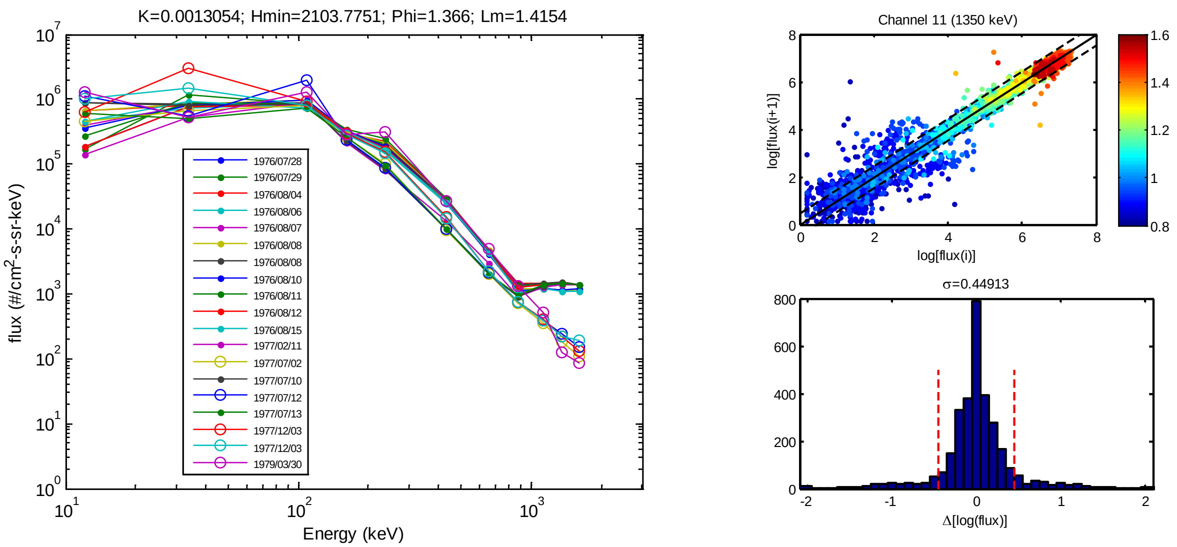

Figure 3. Self-calibration of S3-3 electron channels.

On the left of Figure 3 is an individual energy spectra within one bin for several passes through the bin. Note the two different shapes above approximately 800 keV. On the upper right of Figure 3 is a comparison of flux (at 1350 keV) during one pass versus flux during the subsequent pass. Note the “forks” at low fluxes, which are due to the high energy tails in the energy spectra. **A** histogram of the difference in log flux between successive passes is on the lower right of the figure. The standard deviation is indicated by the dashed red lines, and this is taken as an estimate of the uncertainty in the measurements.

Due to its orbit and instrumentation, the S3-3 spacecraft provided a unique data set for inner-zone electrons. We had hoped to use this data in Version 1.0 of AE9. However, comparisons of S3-3 data with AE8 and other data sets in AE9 showed that fluxes measured by S3-3 were significantly higher than the other data. We therefore investigated why S3-3 might be so different from the other data.

Part of this investigation involved a paper by [33] which contained data from S3-3. In particular, we noted a figure which compared data from S3-3 with other data sets and with AE8 predictions. The data in this figure were processed by A. L. Vampola, the Principal Investigator (PI) on the S3-3 particle detector. The data that we processed for AE9 came from Vampola, and we used software provided by him to process the data. However, in comparing the fluxes from our process to those from the 1994 paper [33], our fluxes are a factor of 10 – 20 higher than those in the paper. Figure 4 illustrates these comparisons where the AES predictions and S3-3 data are shown in black [33]; the S3-3 data in red are from our data analysis (using s33_read) and S3-3 data in green are s33_read fluxes divided by 16. A review of the data processing revealed some small changes between 1994 and the current software. These changes explain slight differences in the spectral shape, but not the factor of 10 – 20. Because we could not explain this discrepancy, we decided to omit the S3-3 data from AE9.

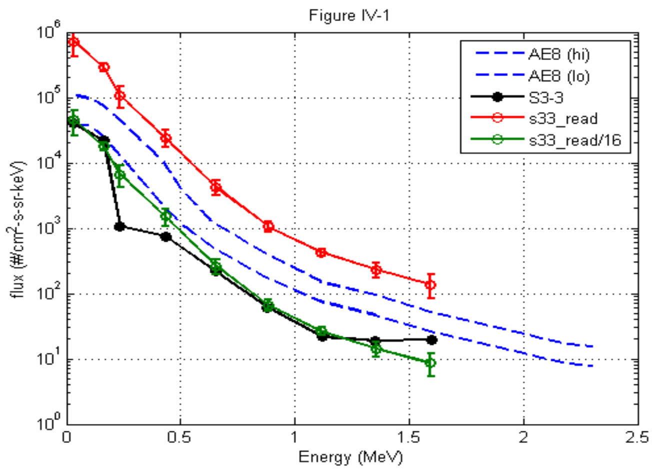

Figure 4. Comparison of S3-3 electron data.

Processing Polar IPS Proton Data

The Imaging Proton Sensor (IPS) on the Polar spacecraft provides data on proton fluxes from approximately 0.01 MeV to 2.0 MeV. The highly elliptical polar orbit covers almost the entire trapped radiation region. Processing included:

- Writing MATLAB routines to read the binary data files and merge them with adiabatic invariant data calculated by AFRL.
- Performing "data cleaning" to identify potential sources of contamination, remove noise from the data, and identify any other issues.
- Mapping fluxes in adiabatic invariant coordinates. Figure 5 contains an example of these maps.

A major part of the Polar data processing involved cross-calibration with other detectors. The cross-calibration was done with the EPAM instrument on the ACE spacecraft and the MICS instrument which was also on the Polar spacecraft. These two instruments overlapped with the upper and lower energy ranges of IPS, respectively. The cross-calibration process revealed some contamination issues where higher energy protons were contaminating the lower energy proton measurements. After filtering out these contaminated measurements, the IPS data agreed well with both MICS and EPAM over the energy range 0.05 – 2.0 MeV. Figure 6 shows a comparison between IPS and EPAM. The cross-calibration also allowed us to estimate measurement errors in the IPS data.

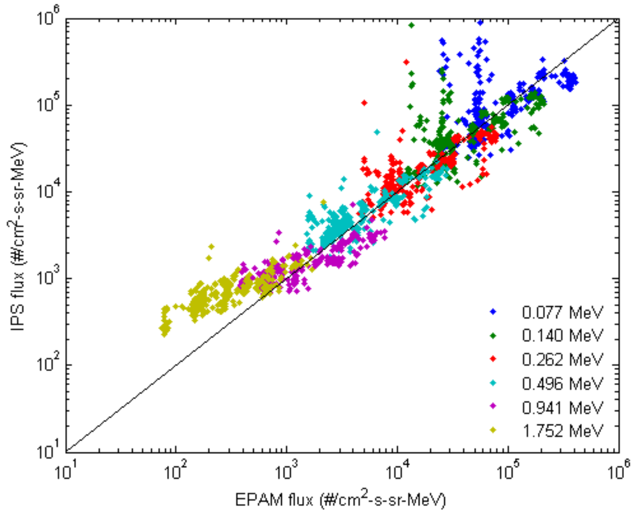

Figure 5. Cross plot of Polar/IPS fluxes vs. ACE/EPAM fluxes at six different energies.

3.2.3 Spectral Inversion Techniques. Our previous spectral inversions, necessary to derive differential flux from detectors with wide energy response, used an assumed spectral function with a power-law spectrum from 10-100 MeV and an exponential tail above 100 MeV. This spectral shape was based on the AP8 model, but it involved parameters which were somewhat arbitrary. Another approach, based on Principal Component Analysis (PCA) proved useful in inverting electron spectra, so a similar approach was developed for protons. The approach was based on an analytical model by Selesnick [34] and covers energies from 10-1000 MeV. Principal components were derived from Selesnick's model and were used to obtain spectra from the TSX5/CEASE data set. Figure 6 shows an example of spectra obtained from the PCA model (blue) and the previous analytical model (red). Dashed lines indicate confidence limits. Inversions based on the PCA approach give slightly better agreement with the data, and this approach was used to re-do the spectral inversions for the TSX5/CEASE data set, as well as other data, for the Version 1.0 release of AP9.

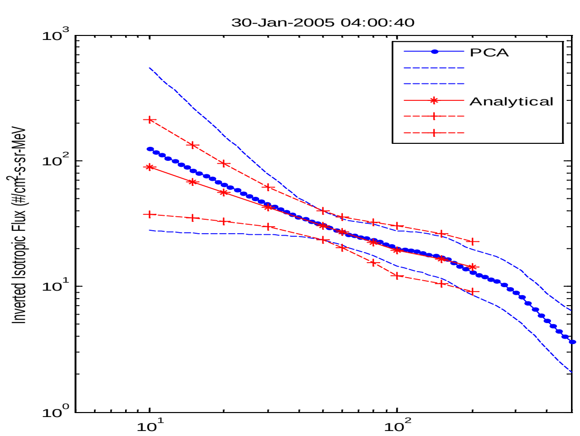

Figure 6. Comparison of spectral inversions of TSX5/CEASE using PCA approach and analytical approach.

Further improvements were made to the PCA model to extend the energies to as low as 5 MeV. These improvements were made to enable the model to be used for spectral inversion of data from other instruments on the HEO spacecraft. MATLAB scripts were developed to use the PCA model to perform spectral inversion of this data. These scripts were transferred to AFRL personnel to perform the actual inversions.

Combined Spectral/Angular Inversion.

The flux maps produced for AE9/AP9 map, the flux of locally-mirroring particles at a given location. Many detectors (including TSX5/CEASE) have a wide acceptance angle and thus measure a wide range of particle pitch angles. Therefore, a method is required to estimate j_{90} from the wide-angle response. Our previous inversions used an after-the-fact approach in which the energy inversion was performed first, then a correction factor was calculated by integrating an assumed particle angular distribution with the known angular response of the detector. This approach was an approximation, but it had the advantage that we were able to determine where large corrections were necessary.

In preparing to perform new inversions for Version 1 of the model, we developed an approach which calculated an effective response function for each detector channel calculated by integrating the assumed particle angular distribution with the known angular response of the detector. This integration was done before the spectral inversion and in principle should result in more accurate fluxes. In reality, however, this process resulted in many instances where no inversion was obtained because the effective response function significantly changed the energy range of the detector. It was therefore decided not to use this approach for the next round of inversions.

We re-visited the approach after the release of Version 1.0; at that time we were able to develop improved pitch angle distribution models and modify the inversion routines to make better use of the effective response functions. At that time, progress was made towards developing a procedure to perform combined spectral and angular inversions of wide-angle detector data. Proton pitch angle distributions (PADs) were developed based on the AP-9 model and MATLAB functions were developed to integrate the ambient PAD with the angular response of the detector to obtain an effective response function which can be used in the inversion procedure. Several integration procedures were investigated; eventually a very simple procedure using the rectangular rule was selected, primarily because speed is an essential feature. The integration functions still need to be tested and integrated with the rest of the inversion procedures.

3.2.4 Development of Flux Templates. In populating the run-time data tables for the AE-9/AP-9 models, individual data sets are combined into one data base. None of these individual data sets covers the full spectral or spatial extent of the final model. In order to perform better interpolation and extrapolation of the data sets, we are developing a series of flux templates which specify how we expect the flux to vary as a function of energy and space.

Flux templates are being developed based on a combination of spacecraft. One of the challenges is extrapolating to regions where data do not exist. This has been accomplished by fitting a sum of exponential functions to the energy spectrum in each bin. The exponentials allow reasonable extrapolation in the energy domain. The fitting parameters are then smoothed in the spatial domain, allowing a more reasonable spatial extrapolation. The smoothed parameters are then used to generate flux maps at the AP-9 energies; these constitute the templates. Figure 7 shows an example of a template. Dots indicate where data were available.

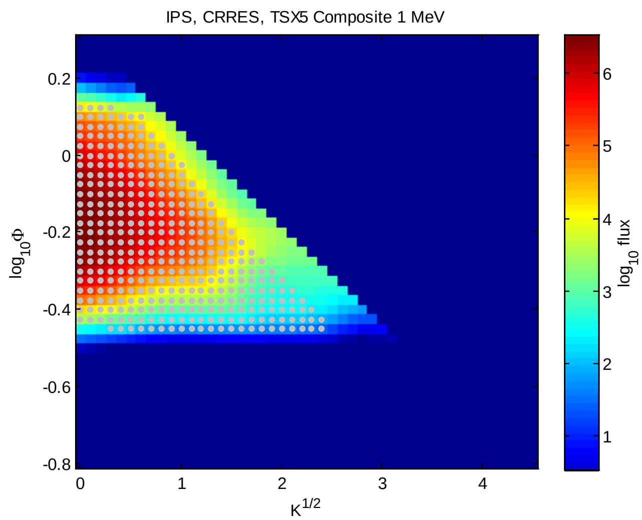

Figure 7. Template mapping proton flux at 1 MeV based on a composite of 3 spacecraft.

3.2.5 TacSat4. TacSat4 (Tactical Satellite 4) is a small spacecraft launched by NRL in September 2011; it carries a CEASE instrument similar to that on TSX5. The data from this instrument will be very useful in updating the flux maps in AE9/AP9. We are working with Dr. Chad Lindstrom at AFRL in performing spectral inversion on the CEASE data. One issue is that in order to extend the inversions to lower energies (down to about 1 MeV), we are including several channels with complicated response functions. Figures 8 and 9 show the response of one of these channels to both 'hard' and 'soft' energy spectra. Red curve (left axis) shows the input proton spectrum. Blue curve (right axis) shows the channel response function for isotropic fluxes. Green bar indicates the energy range representing 80% of the total counts; vertical tick shows the effective midpoint energy. It can be seen that the main response of these channels is highly dependent on the spectral shape.

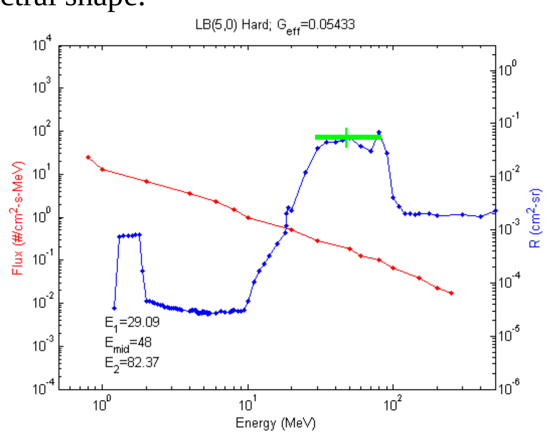

Figure 8. Response of one TacSat4 CEASE channel to a 'hard' proton spectrum (spectral index ~-1).

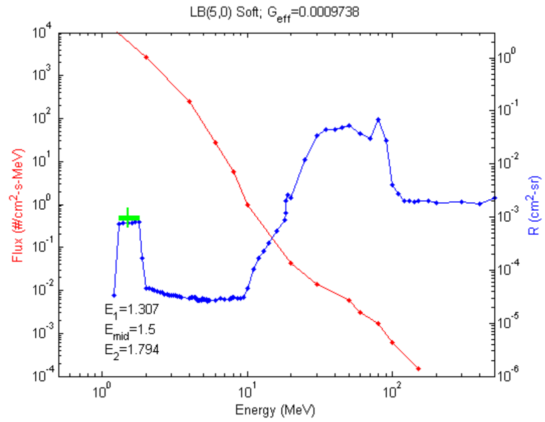

Figure 9. Response of one TacSat4 CEASE channel to a ‘soft’ proton spectrum (spectral index ~-4).

Additional work continued using TacSat-4 data. The following summarizes these efforts:

- One issue is that in order to extend the inversions to lower energies (down to about 1 MeV), we are including several channels with complicated response functions. These channels respond to both low-energy protons and high-energy protons. We developed a criterion based on count rates in two different channels to tell us when the detector was indeed responding to low-energy (< 10 MeV) protons. Figure 10 illustrates this criterion; in general, CEASE responds to < 10 MeV protons beyond L_m ~ 1.8, i.e., in the “slot” region. This criterion will greatly improve our ability to interpret the CEASE data.

- *TacSat-4 Flux Comparisons*. In January and March 2012, a pair of moderate solar particle events (SPEs) occurred. These events are useful for the calibration of proton detectors because they bathe the outer magnetosphere (beyond L_m ~ 6.6) in a relatively uniform flux of medium- to high-energy protons. The GOES spacecraft in geosynchronous orbit are an accepted standard for measuring these SPEs; detectors on TSX5, HEO, and other non-geosynchronous spacecraft have been cross-calibrated against GOES in the past by studying “conjunctions” when the individual spacecraft are at high altitude and/or high latitude. We performed a similar analysis for TacSat-4/CEASE. Figure 11 shows energy spectra from GOES and CEASE; the agreement is quite good. This result gives us confidence in the absolute magnitudes of the proton fluxes derived from CEASE measurements.

- *TacSat-4 Attitude Determination.* The proton fluxes in Earth orbit are typically very anisotropic; for most detectors it is therefore critical to know the look angle of the sensor relative to the magnetic field. For TacSat-4, the CEASE detector looks in the –X direction in spacecraft body coordinates. In order to determine the look direction in magnetic coordinates, it is necessary to use quaternions supplied in the spacecraft attitude control system (ACS) data files; these calculations provide the look direction in inertial coordinates. This vector can then be combined with a magnetic field vector determined by a magnetic field model to determine the pitch angle of the detector boresight. We developed MATLAB routines to read the ACS data files, perform the necessary calculations, and merge the pitch angle data with the CEASE flux data.

- *TacSat-4 Pitch Angle Distributions.* TacSat-4's orbit takes it through essentially the same regions of space several times per day. Over the first several months of data the pitch angle in a given spatial "bin" has varied over a range of about 10 to 90 degrees. It has therefore been possible to generate nearly complete pitch angle distributions (PADs). Figure 12 shows a set of PADs at several energies in one bin near the magnetic equator. These PADs can then be integrated to determine the omnidirectional flux for direct comparison to AP9.

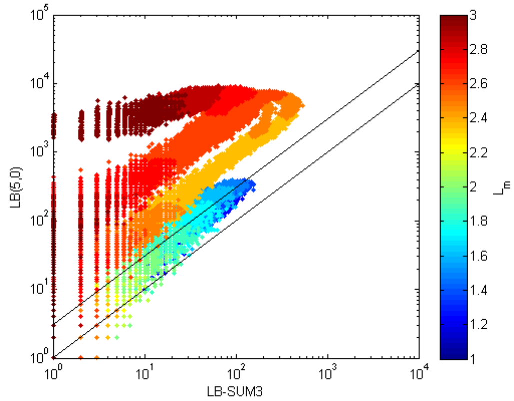

Figure 10. Plot of count rates in CEASE LB(5,0) vs. LB-SUM3.

When LB(5,0) is more than 2 x LB-SUM3 (indicated by upper diagonal line), CEASE channels are responding to < 10 MeV protons. Color scale indicates McIlwain L value of measurements.

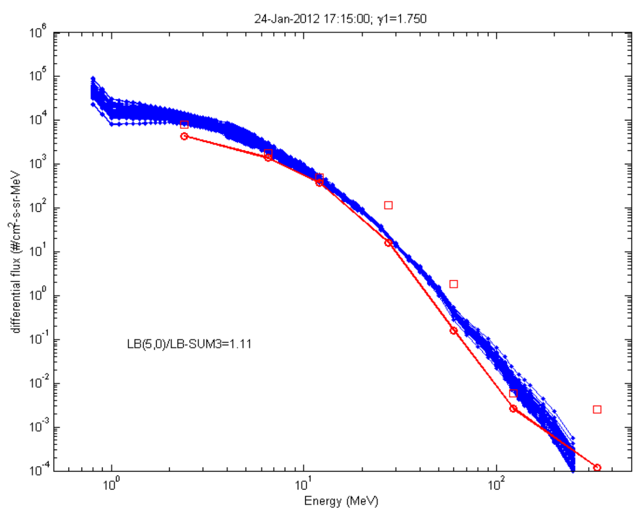

Figure 11. Comparison of CEASE proton fluxes (blue) with fluxes measured by GOES-13 during SPE in January 2012.

Red squares indicate uncorrected GOES fluxes; red circles/line indicate GOES flux corrected for spectral response.

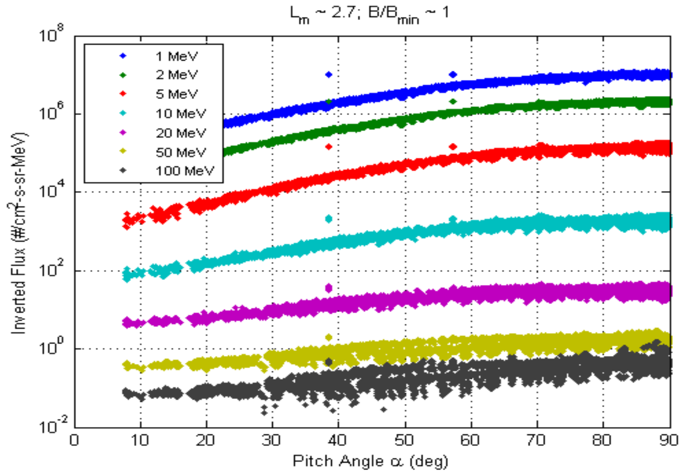

Figure 12. Pitch angle distributions obtained from CEASE Oct 2011 through May 2012.

- *TacSat-4 omnidirectional daily fluences.* Data from the CEASE instrument on TacSat-4 has been used to model the response of solar arrays to the space environment. In order to drive the solar array response models, it was necessary to determine daily omnidirectional proton fluences from the CEASE data.

  The determination of daily omnidirectional fluences was complicated by several factors:
  - The spectral inversion technique used on CEASE determines a unidirectional flux which reflects the average over the CEASE opening angle and near the pitch angle of particles entering along the detector boresight. Some way is needed to estimate the full omnidirectional flux from these measurements.
  - There are gaps in the telemetered data; these gaps may last from a few minutes to a large fraction of a day. On days where there are significant gaps, it is impossible to determine a true daily fluence, and a method for filling the gaps is required.

  Given these factors, it would not be possible to determine accurate omni-directional fluxes or fluences from the CEASE data directly. Fortunately, there are other factors working in our favor:
  - Over the course of six months or so, the proton fluxes in most locations remained relatively stable.
  - Over this time period, due to orbital mechanics and the pointing scheme for TacSat-4, in most bins the CEASE boresight covered a range of pitch angles sufficient to obtain an approximate pitch angle distribution.

A procedure was developed which fills in gaps in the data with the average omni-directional flux in the appropriate bins. The primary assumption involved is that the pitch angle distribution in a given bin on a given day matches the average pitch angle distribution (averaged over the entire period of study) in that bin. This procedure was used to determine daily fluences for the first six months of the mission. Figure 13 shows the average daily flux of 50 MeV protons mapped in K-Φ space for one day of the mission. Superimposed on the flux map is the spacecraft ephemeris.

The color code indicates the daily average flux of 50 MeV protons. The black lines show the TacSat-4 ephemeris for that day. Note the high fluxes for $\log_{10}\Phi$ -0.3. These are due to an ongoing solar proton event.

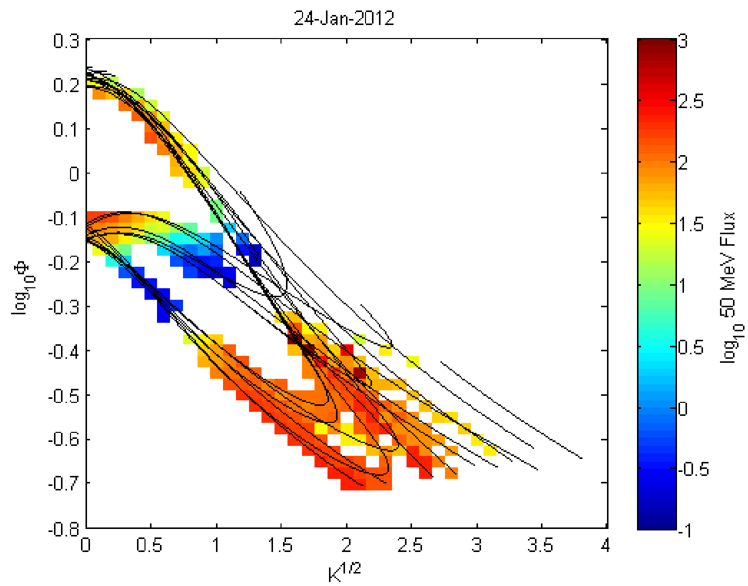

Figure 13. Daily average fluxes for 24 January 2012.

- *TacSat-4 Data Analysis.* In addition to the work described above, some more detailed analysis of the TacSat-4/CEASE data was performed. Figure 14 compares energy spectra measured by TacSat-4 with AP9 model predictions and some of the raw data which went into AP9. It can be seen that TacSat-4 measurements agree reasonably well with AP9 for energies above about 20 MeV and below 2 MeV. In between, however, TacSat-4 measurements are considerably higher than AP9 or the other data sets. For example, at 4.3 MeV, TacSat-4 is about 15 times higher than CRRES and 6 times higher than AP9.

  Figure 15 shows L-profiles (at the magnetic equator) for CRRES data, the AP9 model, and TacSat-4. Again, TacSat-4 is considerably higher than CRRES or AP9.

  Figure 16 shows time histories of the count rate in several CEASE channels which respond to < 10 MeV protons. Also shown is a fit to the trend for the LB-B32 channel, which responds to 2.5 – 4 MeV protons. There is a definite decrease in the count rate (and hence the flux) over time. Based on the inverted flux data, the flux 0f 4.3 MeV protons decreased by about 33% over the course of six months. Extrapolating this rate of decrease, the TacSat-4 flux would reach the levels measured by CRRES in about 3.5 years. Thus, it may be that TacSat-4 is measuring a long-lived transient event. Continued monitoring by TacSat-4, combined with measurements from additional spacecraft, such as TWINS and RBSP, would be very useful in explaining this phenomenon.

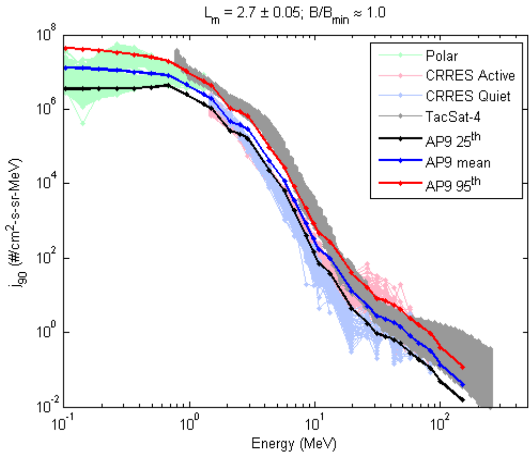

Figure 14. Energy spectra from Polar/IPS, CRRES/Protel, TacSat4, and AP9 in one bin near the magnetic equator.

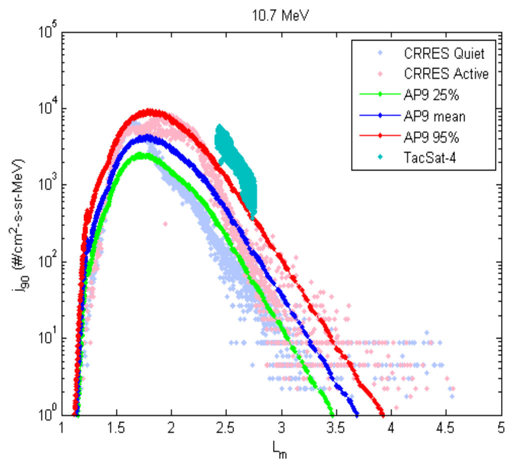

Figure 15. L-profiles of 10.7 MeV flux measured by CRRES and TacSat4, compared with AP9 predictions.

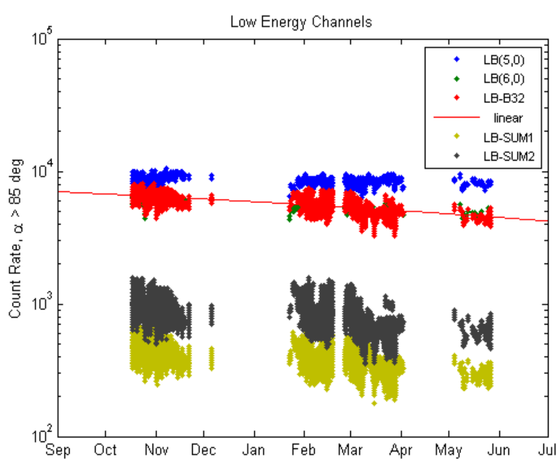

Figure 16. Time history of count rates in several TacSat4/CEASE low energy channels.

AP9 Pitch Angle Distributions. For our next release of AE9/AP9, we are planning to include data from TacSat-4/CEASE and to re-process data from TSX5/CEASE using a combined angular/energy inversion technique which includes both the angular response and the energy response of the instrument. In order to do so, we need a model of the pitch angle distribution of the ambient proton flux. We have used the directional flux capability of AP9 to derive pitch angle distributions as a function of McIlwain L parameter and energy. Figure 17 shows an example of the pitch angle distributions at a number of energies at L_m=1.5. Here, y=sinα_{eq}, where α_{eq} is the equatorial pitch angle, and y_{LC} is the value of y corresponding to the loss cone. These pitch angle distributions have been tabulated and will be included in updated inversion procedures for processing future data from CEASE and other detectors.

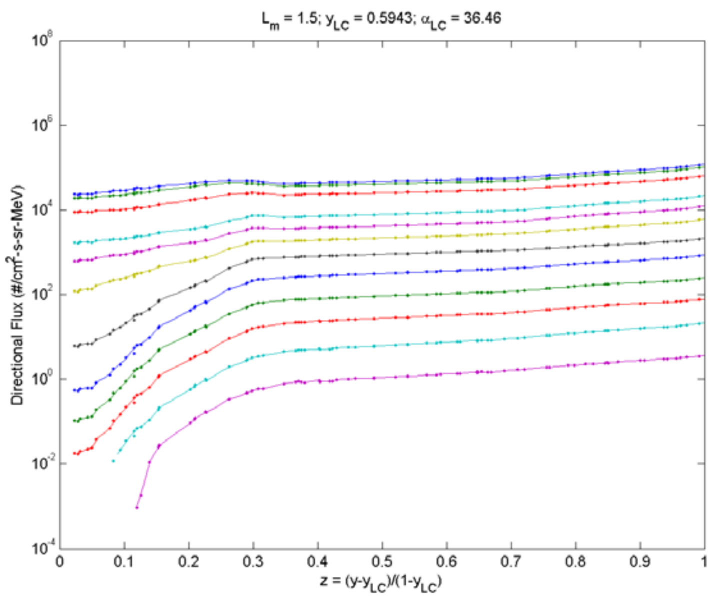

Figure 17. Pitch angle distributions derived from AP9 for L_m=1.5.

3.2.6 Solar Particle Event Database. In analyzing data for AE9/AP9, we have attempted to remove data taken during solar particle events (SPEs), because the high energy protons present during these events can contaminate measurements. We have been using two different event lists based on GOES data, one for > 100 MeV protons and one for > 10 MeV protons. These lists contained events from 1986 through 2006. Some of the AE9/AP9 data, however, were taken before 1986, and new data (e.g., the TacSat-4 data) are being taken. In order to develop a relatively consistent list of events, a new list has been compiled. This list is based primarily on the SEPEM data set (http://dev.sepem.oma.be/) which contains data from 1973 through 2006. The SEPEM list is slightly different in that it uses the differential flux in the 7.23 - 10.46 MeV channel, while the previous list used integral fluxes in a > 10 MeV or > 100 MeV channel. Comparisons of the two lists showed that almost all the events in one list were contained in the other; timings of the events were slightly different. The SEPEM list was updated with data from GOES for 2007 – 2012. A MATLAB data set was created and a MATLAB function was written to return a flag indicating whether or not a SPE was in progress at a given time.

3.2.7 Relativisitic Electron Prediction Models Comparisons. Extended periods of relativistic electron intensity at geosynchronous orbit can create severe deepcharging hazards for satellites. Over the last 20 years a number of models have been developed to predict electron flux levels using solar wind and geomagnetic indices as inputs. We analyze the results of several of these including the Relativistic Electron Forecast Model based on the linear prediction filter technique, a neural network algorithm, and the physics based diffusion method. Analyses using the methods of simple persistence and recurrence (based on the 27 day solar rotation) are also included as performance baselines. Comparisons are made to the GOES> 2MeVelectron flux to determine which model or method gives the best +1, +2, and +3 day forecasts of average daily flux during the interval 1996–2008. Model inputs include combinations of SKp, the daily average solar wind speed, and daily average > 2 MeV electron fluxes for one day or multiple days prior to the forecast days of interest. Prediction efficiencies are calculated for 6 month intervals. After evaluating all the models, there was no clear winner; each model did well at different phases of the solar cycle. All models perform their best during the inclining phase of solar minimum but not as well during solar maximum and the declining phase of solar minimum. While persistence is respectable for +1 day prediction, models clearly give superior +2 and +3 day predictions and should be used to obtain those forecasts. The results of this study were published is the Space Weather Journal [35].

3.3 AFGEOSpace Development

One of our goals under this contract was to contribute to the maintenance of AFGEOSpace2.5 and to the new version AFGEOSpace3.0.

AF-GEOSpace is a user-friendly, graphics-intensive software program bringing together many of the space environment models, applications, and data visualization products developed by the Air Force Research Laboratory and others in the space weather community. AF-GEOSPACE currently serves as a platform for rapid prototyping of operational products, scientific model validation, environment specification for spacecraft design, mission planning, frequency and antenna management for HF communications, and post-event anomaly resolution.

AF-GEOSpace provides common input data sets, application modules, and 1-D, 2-D, and 3-D visualization tools to all of its models. Available graphical tools include animation, annotation, axes, coordinate probes, coordinate slices, detector cones (e.g., from satellites), Earth, emitters (e.g., radar fans and communication domes), field-lines (e.g., geomagnetic), global inputs (e.g., Kp and Dst indices), grids, isosurfaces, links (e.g., ground-to-satellite), orbit probe (data along orbit tracks), orbit slice (data in orbit plane), plane slice (data in arbitrary plane), ray trace (through ionosphere electron densities), satellites, stars, stations, and volume (global 3-D rendering of data sets). The software's "dynamic" mode enables the simultaneous display of output from multiple environment models as a function of time over user-specified intervals.

Boston College efforts to support AFGEOSpace 2.5 primarily included programming, bug fixing, graphics development, resolving differences on program results between operating systems, library testing and responding to AFRL requests for clarification and further developments. One of the problems with this and earlier versions of AFGEOSpace were that each new component model and its accompanying GUI needed to be compiled directly into AFGEOSpace. This required the entire AFGEOSpace program to be updated when a single component model was added. Similarly, when models or their interface were revised, the entire AFGEOSpace program had to be updated. During the course of this contract, BC expended much support to improve these issues in the development of AFGEOSpace Version 3.0. These efforts included contributing to the development of a modular approach with plug-ins created using dynamic linked libraries for Windows users or shared libraries for Linux and OSX users. These changes allowed AFGEOSpace 3.0 to dynamically load the module at runtime and when a component model is changed, AFGEOSpace needs only to be restarted to observe the changes. Since the models are loaded at runtime only those models of interest to the user are required. AFGEOSpace Version 3 also incorporated a platform independent graphical user interface (GUI). That is created in an external program and then stored as an XML file. This XML file is then loaded by AFGEOSpace when the plug-in module is loaded. Since the XML file is a plain text description of the GUI, it is platform independent and only one XML file is needed to work on Windows, Linux or OSX.

All of our efforts for AFGEOSpace 2.5 and 3.0 were coordinated with other the AFRL program manager for AFGEOSpace and with other AFRL contractors.

Some of the work addressed by Boston College included:

- Development on an interface builder. This program allows programmers to interactively build GUI's for their plug-ins for AFGEOSpace. A "plug-in" is a code library that is dynamically loaded into AFGEOSpace at runtime.
- Implementing window creation and creating a menu bars
- Updating the GUI for the SNRTACS model.
- GuiBuilder (program that allows user to build interfaces)
- Fixed issues when loading a previously saved file objects would not appear correctly.
- Various debugging to the driver for the SNRTACS model
- SNRTACS model discrepancies when run on Windows and Linux operating systems
- Fixes to the EPHEMERIS model and corresponding graphical display
- METEOR IMPACT: Open Model not working
- METEOR SKY MAP: Save/Open Model loads GUI settings and the correct data for display, but any entries in the "Storms" box are not retained - thus rerunning the loaded module does not include the missing storm.
- METEOR IMPACT-APP: Open Model not working
- METEOR IMPACT-APP: Freezes with valid Optional Storm added in fresh AF-GEOSpace session. Results in "invalid storm peak" message.
- Raytrace App: Save Model message “AppRayTrace1_Frequency_time_02 Def Dim:0 NC_UNLIMITED size already in use
- Error Message: Model Save 19: NC-UNLIMITED size already in use”
- Open Model message: Error Message: Variable not found
- Viewport Menu: Projection: Attempting to use the Projection option to change the dimension of special 1-D plot windows created by LET-APP, RAYTRACE-APP, and PPS causes crash.
- LET-APP: Use of "Trapped Protons: CRRESPRO Quiet" or "Active" results in no output change and error message.

- Crresele-App: Exceeded NETCDF maximum number of dimensions.
- Changes to the management of the dynamic loading/unloading of libraries. (i.e. ‘plugins’)
- Bug fixes to the display of color plots
- Generating a more unified build environment
- Heliospace changes mainly revolved around completing the implementation of support for 2.5-D data sets. Issues fixed were the proper display of coordinate slices and generation of field lines.
- Corrected bugs that caused crashes in the animation module for Heliospace
- Fixes to get proper graphical display when using multiple overlay planes
- Expanded the 2D plotting graphics to create vertical labeling with proper placement
- Created 2D plot graphing object
- Created satellite grid object and user interface
- updated various models for V3.0 support
- updated the radiation models which involved updating the radiation belt code and creating APEX, CRRES and NASA modules
- updated magfield and SAA models
- developed a new grid module and GUI that supports various coordinate spaces
- updated the satellite grid and GUI

Efforts were finalized on the support updates to various models for V3.0. These updates along with all pertinent information and code were sent to AFRL.

Heliospace Analysis Tools: The Heliospace software package is a unique scientific tool that provides enhanced graphical and data visualization of 3-Dimensional (3D), time-varying systems. The software was developed by Boston College personnel as a fundamental graphics module for the AFGEOSpace space environment program.

The Heliospace package is unique in that it generates 3D adaptive grids for both Cartesian and spherical data sets. In addition, field lines can be generated from vector data and then rendered into 3D grid space. Graphical options include coordinate slices, grid points, isosurfaces and domains. Once rendered the graphics may then be manipulated by rotating, translating and zooming in and out. Multiple viewports can be created to give different views of a single object or to view multiple data sets simultaneously. In addition, time dependent data sets can be viewed in animation.

During the course of this contract, the Heliospace package was enhanced to allow a user to create and playback macros; to create a color map legend; to create a new graphical object to allow the user to add annotations to the image; to improve display options for the data domain; and to allow the user to select the background color and gradient.

3.4 History of the Ring Current

The "ring current" grows in the inner magnetosphere during magnetic storms and contributes significantly to characteristic perturbations to the Earth's field observed at low-latitudes. Work under this contract was expended on writing a short history of the ring current that develops in the Earth's magnetosphere during magnetic storms. This effort resulted in a publication in the History of Geomagnetic and Space Science outlining how understanding of the ring current evolved during the half-century intervals before and after humans gained direct access to space. Its existence was first postulated in 1910 by Carl Størmer to explain the locations and equatorward migrations of aurorae under stormtime conditions. In 1917 Adolf Schmidt applied Størmer's ring-current hypothesis to explain the observed negative perturbations in the Earth's magnetic field. More than another decade would pass before Sydney Chapman and Vicenzo Ferraro argued for its necessity to explain magnetic signatures observed during the main phases of storms. Both the Størmer and Chapman–Ferraro models had difficulties explaining how solar particles entered and propagated in the magnetosphere to form the ring current. During the early 1950s Hannes Alfvén correctly argued that the ring current was a collective plasma effect, but failed to explain particle entry. The discovery of a weak but persistent interplanetary magnetic field embedded in a continuous solar wind provided James Dungey with sufficient evidence to devise the magnetic merging-reconnection model now regarded as the basis for understanding magnetospheric and auroral activity. In the mid-1960s Louis Frank showed that ions in the newly discovered plasma sheet had the energy spectral characteristics needed to explain the ring current's origin [36].

3.5 Second Planar Langmuir Probe

The objective of this effort was to provide engineering services for a number of circuit boards and other elements for space measurements. One of our efforts included investigating the development of the second planar Langmuir probe (SPLP). This included refining the design of the logarithmic amplifier and laying out the printed circuit board for it. The board was mostly laid out when a shortcoming of the operational amplifier to be used was discovered. The amplifier input has to be limited to less than 2.5 volts. The problem was discovered in testing at Kirtland. This necessitated much circuit redesign. The design was coordinated with Kirtland personnel.

Final schematics of the analog board, board layout and parts list for the engineering version of the board needed were prepared for presentation to AFRL. The engineering printed circuit board was ordered and assembled by AFRL and sent to Boston College for testing. Between engineering board design and testing, time was spent on the flight version of the board. The flight version differs in the component footprints. Some commercial components were used for the engineering version of the analog board. They cost a small fraction of the flight quality components. Functionally they are the same but have different packages requiring different printed circuit board footprints. Documentation and shipping of test boards was completed.

Work was also done in collaboration with AFRL, MIT Lincoln Lab (MITLL) and COSMIAC Corporation in the design of a new radiation detector. The new design instrument was to be a small, light weight, low power radiation detector. Integration details between AFRL hardware and the MITLL satellite were completed. The interface rules kept changing as MITLL changed their satellite design.

The new project CEASE Mk3 (Compact Environmental Anomaly Sensor Mark 3) was also addressed under this contract. The Mk3 indicates the third generation of similar instruments. The goal of this instrument is to provide a simple, economical, future parts available, in-house version of the previous generations. The previous versions had many unique and expensive parts. Advances in the electronics will permit use of more common off the shelf parts. A new power supply was designed.

3.6 Data Analysis Center (DAC) Support

While at Hanscom AFB, Boston College team members supported the “Middle Earth” computer cluster and the Stoermer data server for RVBX. All servers utilized Red Hat and CentOS operating systems. Workstations were a mix of Fedora Linux and Microsoft Windows operating systems. Team members performed necessary actions in compliance with all security and network regulations. System performance management was an active and ongoing task. The team also maintained hardware, software, and software licensing. Research of equipment, peripherals, and software was included in the overall consulting effort and recommendations were provided to management for consideration. Lastly, user support demanded a significant portion of the overall effort.

Throughout the BRAC transitional period, Boston College provided primary support at AFRL Hanscom AFB for archiving, cataloging, labeling, and properly packing servers and data storage equipment for the physical move to Kirtland AFB. Upon arrival at Kirtland, BC team members provided ongoing technical (interchange) guidance in support of the successful reassembly of all RVBX servers and data storage equipment into the new data analysis facility. All network communications between servers and storage equipment was reestablished. Operating systems, security and network settings were adjusted for the new base guidelines at Kirtland, and all data was again archived and verified. BC team members worked tirelessly through all challenges presented by the BRAC transition and until all tasks were successfully completed.

4. RESULTS AND DISCUSSION

Since this project consisted of numerous research efforts, we have included the results and discussion for each project in the previous sections.

5. CONCLUSIONS

Under this contract, the Boston College ISR conducted an innovative scientific research and analysis program to understand the fundamental solar and magnetospheric processes and mechanisms that drive and control the Earth’s space environment in order to understand, specify, anticipate and mitigate the effects of space weather on Air Force Systems. As part of our efforts, we supported this program with research and instrument development to study the origins and interplanetary (IP) propagation of disturbances that affect the geosphere and supported the mission and data analysis for the AFRL Solar Mass Ejection Imager (SMEI) experiment, a Heliospheric image/detector that observes and tracks coronal mass ejections from the Sun to Earth. Staff members also contributed to the development of the Space Weather Forecasting Lab (SWFL) at AFRL. Boston College also provided scientific and technical collaboration to AFRL/RVB to aid and enable the development and validation of the AE-9 and AP-9 models, the next-generation of trapped electron and proton models designed to replace the current AE-8 and AP-8 models and provide users with much-needed improvements in accuracy and additional capabilities. This work also addressed the development of enhanced versions of AFGEOSpace and the Heliospace analysis toolset. Finally, special projects in support of Earth's Space environmental studies were addressed throughout the duration of the contract. These include the use and analysis of various space sensors and satellite missions, and the development of Stoermer as the primary data file server for RVBX. Numerous presentations were made at national and international conferences. At least 20 papers were published in peer reviewed journals.

REFERENCES

[1] Webb, D. F., S. E. Gibson, and B. J. Thompson, "Whole Heliosphere Interval: Overview of JD16," in Highlights of Astronomy, Vol. 15, IAU, I.F. Corbett, ed., Cambridge Univ. Press, 2010.

[2] Gibson, S. E., D. F. Webb, and B. J. Thompson, "The Whole Heliosphere Interval in the context of the current solar minimum," ASP Conference Series, Vol. 428, p. 223, S. R. Cranmer, J. T. Hoeksema, and J. L. Kohl (eds.), 2010.

[3] Gibson, S. E., G. de Toma, B. Emery, P. Riley, L. Zhao, Y. Elsworth, R. J. Leamon, J. Lei, S. McIntosh, R. A. Mewaldt, B. J. Thompson, and D. Webb, "The Whole Heliosphere Interval in the Context of a Long and Structured Solar Minimum: An Overview from Sun to Earth," WHI SI, *Solar Phys.,* 2011.

[4] Thompson, B. J., et al., "A Snapshot of the Sun Near Solar Minimum: The Whole Heliosphere Interval," WHI SI, *Solar Phys.,* 274, pp. 29-56, 2011.

[5] Webb, D. F., H. Cremades, A. C. Sterling, C. H. Mandrini, S. Dasso, S. E. Gibson, D. A. Haber, R. W. Komm, G. J. D. Petrie, P. S. McIntosh, B. T. Welsch, and S. P. Plunkett, "The Global Context of Solar Activity During the Whole Heliosphere Interval Campaign," *Solar Phys.*, 274, pp. 57-86, 2011.

[6] Webb, David F. and Timothy A. Howard, "Coronal Mass Ejections: Observations," *Living Rev. Solar Phys.* (http://www.livingreviews.org/lrsp-2012-3), 9, 3, 2012.

[7] Jackson, B. V., A. Buffington, P. P. Hick, J. M. Clover, M. M. Bisi, and D. F. Webb, "The 26 April 2008 CME: SMEI 3-D reconstruction of an ICME interacting with a co-rotating solar wind density enhancement," *Solar Phys.,* 724, pp. 829-834, 2010.

[8] Harrison, R. A., J. A. Davies, A. P. Rouillard, C. J. Davis, C. J. Eyles, D. Bewsher, S. R. Crothers, R. A. Howard, N. Sheeley, A. Vourlidas, D. F. Webb, D. S. Brown, and G. Dorrian, "Two years of the STEREO Heliospheric Imagers," *Solar Physics*, 256, pp. 219-237, 2009.

[9] Harrison, R. A., J. A. Davies, C. Möstl, Y. Liu, M. Temmer, M. M. Bisi, J. P. Eastwood, C. A. de Koning, N. Nitta, C. J. Farrugia, R. J. Forsyth, B.V. Jackson, E. A. Jensen, E. K. J. Kilpua, D. Odstrcil, T. Rollett, and D. F. Webb, "An analysis of the onset and propagation of the multiple coronal mass ejection events of 01 August 2010," *Astrophys. J.*, 750, 45, 2012.

[10] Webb, D. F., T. A. Howard, C. D. Fry, T. A. Kuchar, D. Odstrcil, B. V. Jackson, M. M. Bisi, R. A. Harrison, J. S. Morrill, R. A. Howard, and J. C. Johnston, "Study of CME Propagation in the Inner Heliosphere: SMEI and STEREO HI Observations of the January 2007 Events," *Solar Physics*, 256, pp. 239-267, 2009.

[11] Webb, D. F., C. Möstl, B.V. Jackson, M. M. Bisi, T. A. Howard, T. Mulligan, E. A. Jensen, L. K. Jian, J. A. Davies, C. A. de Koning, Y. Liu, M. Temmer, J. M. Clover, C. J. Farrugia, R. A. Harrison, N. Nitta, D. Odstrcil, S. J. Tappin, and H.-S. Yu, "Heliospheric Imaging of 3-D Density Structures During the Multiple Coronal Mass Ejections of Late July to Early August 2010," *Solar Phys, TI: Observations & Modeling of the Heliosphere*, 285, pp. 317-348, 2012.

[12] Webb, D. F., M. M. Bisi, C. A. de Koning, C. J. Farrugia, B.V. Jackson, L. K. Jian, N. Lugaz, K. Marubashi, C. Möstl, E. P. Romashets, B. E. Wood, and H-S Yu, "An ensemble study of a January 2010 CME: Connecting a non-obvious solar source with its ICME/magnetic cloud," *Solar Phys*., submitted, 2014.

[13] Liu, Ying, Janet G. Luhmann, Christian Moestl, Juan Martinez Oliveros, Stuart Bale, Robert P. Lin, Richard A. Harrison, Manuela Temmer, David F. Webb, and Dusan Odstrcil, "Interactions between Coronal Mass Ejections Viewed in Coordinated Imaging and In Situ Observations," *Astrophys. J. Lett.*, 746, L15, 2012.

[14] Möstl, C., C. J. Farrugia, E. K. J. Kilpua, L. K. Jian, Y. Liu, J. P. Eastwood, R. A. Harrison, D. F. Webb, M. Temmer, D. Odstrcil, J. A. Davies, T. Rollett, J. G. Luhmann, N. Nitta, T. Mulligan, E. A. Jensen, R. Forsyth, B. Lavraud, C. A. de Koning, A. M. Veronig, A. B. Galvin, T. L. Zhang, and B. J. Anderson, "Multi-Point Shock and Flux Rope Analysis of Multiple Interplanetary Coronal Mass Ejections Around 2010 August 1 in the Inner Heliosphere," *Astrophys. J*., 758, 10, 2012.

[15] Odstrcil, D., H. Xie, C. A. de Koning, A. P. Rouillard, C. Möstl, M. Temmer, L. K. Jian, M. Dryer, J. A. Davies, C. J. Davis, R. A. Harrison, D. F. Webb, C. N. Arge, and T.-L. Zhang, "Numerical heliospheric simulation as an assisting tool for interpretation of the "first STEREO multi-event," four coronal mass ejections (CMEs) of 2010-08-01," *J. Geophys. Res.*, 2013.

[16] Woods, Thomas N., Rachel Hock, Frank Eparvier, Andrew R. Jones, Phillip C. Chamberlin, James A. Klimchuk, Leonid Didkovsky, Darrell Judge, John Mariska, Harry Warren, Carolus J. Schrijver, David F. Webb, Scott Bailey, and W. Kent Tobiska, "New Solar Extreme Ultraviolet Irradiance Observations During Flares," *Astrophys. J.*, 739, 59, 2011.

[17] Vrˇsnak, B., G. Poletto, E. Vuji´c, A. Vourlidas, Y.-K. Ko, J. C. Raymond, A. Ciaravella, T. ˇZic, D. F. Webb, A. Bemporad, F. Landini, G. Schettino, C. Jacobs, and S. T. Suess, "Morphology and density structure of post-CME current sheets," *A&A*, 499, pp. 905-916, 2009.

[18] Ciaravella, A., D. F. Webb, S. Giordano, and J. C. Raymond, "Bright Ray-like Features in the Aftermath of CMEs: White Light vs UV Spectra," *Astrophys. J.*, 766, 65, 2012.

[19] Webb, D. F., "Eruptive Current Sheets Trailing CMEs; Results from LASCO," *Astrophys. J.*, to be submitted, 2014.

[20] Kahler, S. W. and D. F. Webb, "Tracking Nonradial Motions and Azimuthal Expansions of Interplanetary CME with the Solar Mass Ejection Imager," Proc. of Solar Wind 12 Workshop, AIP, 1216, pp. 408-411, 2010.

[21] Mizuno, D., A. Buffington, M. P. Cooke, C. J. Eyles, P. P. Hick, P. E. Holladay, B. V. Jackson, J. C. Johnston, T. Kuchar, J. B. Mozer, S. Price, R. R. Radick, G. M. Simnett, D. Sinclair, J. Tappin, and D. F. Webb, "Very High-Altitude Aurora Observations With the Solar Mass Ejection Imager," *J. Geophys. Res.*, 110, A7, A07230, 2005.

[22] Kuchar, T. A., A. Buffington, C. N. Arge, P. P. Hick, T. A. Howard, B. V. Jackson, J. C. Johnston, D. R. Mizuno, S. J. Tappin, and D. F. Webb, "Observations of a Comet Tail Disconnection Induced by CME Passage," *J. Geophys. Res.*, A04101, 2008.

[23] Hounsell, R., M. F. Bode, P. P. Hick, A. Buffington, B. V. Jackson, J. M. Clover, A. W. Shafter, M. J. Darnley, N. R. Mawson, I. A. Steele, A. Evans, P. S. Eyres, and T. J. O'Brien, "Exquisite Nova Light Curves from the Solar Mass Ejection Imager (SMEI)," *Astrophys. J.*, 724, pp. 480-486, 2010.

[24] Mizuno, Donald R., Stephan D. Price, Kathleen E. Kraemer, Thomas A. Kuchar, and Janet C. Johnston, "Debris swarms seen by SMEI," *Adv. Space Res.*, 49, pp. 162-176, 2012.

[25] Howard, T. A., M. M. Bisi, A. Buffington, J. M. Clover, M. P. Cooke, C. J. Eyles, P. P. Hick, P. E. Holladay, B. V. Jackson, J. C. Johnston, S. W. Kahler, T. A. Kuchar, D. R. Mizuno, A. J. Penny, S. D. Price, R. R. Radick, G. M. Simnett, S. J. Tappin, N. R. Waltham, and D. F. Webb, "The Solar Mass Ejection Imager and Its Heliospheric Imaging Legacy," *Space Sci. Rev.*, 180, pp. 1-38, 2013.

[26] Webb, D. F., T. A. Howard, C. D. Fry, T. A. Kuchar, D. R. Mizuno, J. C. Johnston, and B. V. Jackson, "Studying Geoeffective ICMEs between the Sun and Earth: Space Weather Implications of SMEI Observations," *Space Weather*, 7, 2009.

[27] Howard, T. A. and S. J. Tappin, "The Application of a New Phenomenological Coronal Mass Ejection Model to Space Weather Forecasting," *Space Weather*, 8, S07004, 2010.

[28] Webb, D. F., J. C. Johnston, T. A. Kuchar, J. Tappin, and T. A. Howard, SH54D-05: "Forecasting Earth Arrivals of CMEs with Heliospheric Imagers," (Invited), p. 557, AGU Fall Meeting Program, 13-17 August 2010.

[29] Davis, C. J., C. A. de Koning, J. A. Davies, D. Biesecker, G. Millward, M. Dryer, C. Deehr, D. F. Webb, K. Schenk, S. Freeland, C. Möstl, and C. J. Farrugia, "A comparison of Space Weather analysis techniques used to predict the arrival of the Earth-directed CME and its shockwave launched on 8 April 2010," *Space Weather*, 9, S01005, 2011.

[30] Webb, David F., "Coronal Mass Ejections and Space Weather," in *ASI Conference Series of the Bulletin of the Astronomical Society of India*, Eds: P. B. Rao, N. Gopalswamy, S. S. Hasan, and P. Subramanian, Vol. xx, in press, 2014.

[31] Gopalswamy, N., J. M. Davila, O. C. St. Cyr, T. Duvall, E. Sittler, R. J. MacDowall, A. Szabo, M. Collie, J. Johnston, D. F. Webb, E. W. Cliver, S. W. Kahler, F. Auchère, M. Maksimovic, J.-L. Bougeret, B. Heber, S. Vennerstrom, C. de Koning, D. Biesecker, V. Pizzo, R. L. Moore, A. Sterling, A. Vourlidas, R. A. Howard, J. Zhang, B. Vrsnak, and P. Rajaguru, "Earth-Affecting Solar Causes Observatory (EASCO): A New View from Sun-Earth L5," *Decadal Survey White Paper*, Nov. 2010

[32] Vourlidas, A., R. Howard, Y.-K. Ko, D. Biesecker, S. Krucker, M. Thomson, T. Bogdan, C. St Cyr, J. Davila, G. Doschek, N. Gopalswamy, C. Korendyke, M. Laming, P. Liewer, R. Lin, S. Plunkett, D. Socker, S. Tomczyk, and D. Webb, "Mission to the Sun-Earth L5 Lagrangian Point: An Optimal Platform for Heliophysics & Space Weather Research," *Decadal Survey White Paper*, Nov. 2010

[33] Abel, R., R. M. Thorne, and A. L. Vampola, "Solar cyclic behavior of trapped energetic electrons in Earth's inner radiation belt," *J. Geophys. Res*., 99, A10, pp. 19,427-19,431, 1994.

[34 Selesnick, R. S., M. D. Looper, and R. A. Mewaldt, "A theoretical model of the inner proton radiation belt," *Space Weather*, 5, S04003, doi:10.1029/2006SW000275, 2007.

[35] Perry, K. L., G. P. Ginet, A. G. Ling, and R. V. Hilmer, "Comparing geosynchronous relativistic electron prediction models," *Space Weather*, 8, S12002, doi:10.1029/2010SW00058, 2010.

[36] Egeland, A. and W. J. Burke, "The Ring Current: A Short Biography," *Hist. Geo- and Space Sci*., Vol. 3, Issue 2, pp 131-142, 2012.

APPENDIX – Publications and Presentations

Publications

Davis, C. J., C. A. de Koning, J. A. Davies, D. Biesecker, G. Millward, M. Dryer, C. Deehr, D. F. Webb, K. Schenk, S. Freeland, C. Möstl, and C. J. Farrugia, "A comparison of Space Weather analysis techniques used to predict the arrival of the Earth-directed CME and its shockwave launched on 8 April 2010," *Space Weather,* Vol. 9m S01005, doi: 10.1029/2010SW000620, 2011.

Egeland, A. and W. J. Burke, "The Ring Current: A Short Biography," *Hist. Geo- and Space Sci*., Vol. 3, Issue 2, pp. 131-142, 2012.

Gibson, S.E., D. F. Webb, and B. J. Thompson, "The Whole Heliosphere Interval in the context of the current solar minimum," ASP Conference Series, Vol.428, p. 223, S. R. Cranmer, J. T. Hoeksema, and J. L. Kohl (eds.), 2010.

Gibson, S. E., G. de Toma, B. Emery, P. Riley, L. Zhao, Y. Elsworth, R. J. Leamon, J. Lei, S. McIntosh, R. A. Mewaldt, B. J. Thompson, and D. Webb, "The Whole Heliosphere Interval in the Context of a Long and Structured Solar Minimum: An Overview from Sun to Earth," WHI SI, *Solar Phys.*, 2011.

Ginet, G., S. L. Huston, D. Madden, C. J. Roth, and T. P. O'Brien, "The Trapped Proton Environment in Medium Earth Orbit (MEO)," *IEEE Transactions on Nuclear Science*, Vol. 57, 6, 2010.

Jackson, B. V., A. Buffington, P. P. Hick, J. M. Clover, M. M. Bisi, and D. F. Webb, "The 26 April 2008 CME: SMEI 3-D reconstruction of an ICME interacting with a co-rotating solar wind density enhancement," *Solar Phys.,* 724, pp. 829-834, 2010.

Kuchar, T.A., A. Buffington, C. N. Arge, P. P. Hick, T. A. Howard, B. V. Jackson, J. C. Johnston, D. R. Mizuno, S. J. Tappin, and D. F. Webb, "Observations of a Comet Tail Disconnection Induced by CME Passage," *J. Geophys. Res.*, A04101, 2008.

Ling, A. G., G. P. Ginet, R. V. Hilmer, and K. L. Perry, "A neural network-based geosynchronous relativistic electron flux forecast model," *Space Weather,* 8, S09003, doi: 10.1029/2010SW000576, 2010.

Maynard, N. C., C. J. Farrugia, W. J. Burke, D. M. Ober, F. S. Mozer, H. Rème, M. Dunlop, and K. D. Siebert, "Cluster observations of the dusk flank magnetopause near the sash: Solar wind/IMF control, ion dynamics, and flow through reconnection," *J. Geophys Res*., Vol 116, A1, doi: 10.1029/2010JA015872, 2011.

Mizuno, D. R., S. D. Price, K. E. Kraemer, T. A. Kuchar, and Janet C. Johnston, "Debris swarms seen by SMEI," *Adv. Space Res.*, 49, pp. 162-176, 2012.

Perry, K. L., G. P. Ginet, A. G. Ling, and R. V. Hilmer, “Comparing geosynchronous relativistic electron prediction models,” *Space Weather*, 8, S12002, doi:10.1029/2010SW00058, 2010.

Thompson, B. J., S. E. Gibson, P. C. Schroeder, D. E. Webb, C. N. Arge, M. M. Bisi, G. de Toma, B. A. Emery, B.A., A. B. Galvin, D. A. Haber, B. V. Jackson, E. A. Jensen, R. J. Leamon, Lei Jiuhou P. K. Manoharan, M. L. Mays, P. S. McIntosh, G. J. D. Petrie, S. P. Plunkett, Qian Liying, P. Riley, S. T. Suess, M. Tokumaru, B. T. Welsch, and T. N. Woods, (2011), “A Snapshot of the Sun Near Solar Minimum: The Whole Heliosphere Interval,” *Solar Phys.* Vol. 274, Numbers 1-2, pp. 29-56, DOI: 10.1007/s11207-011-9891-6, 2011.

Webb, D. F., H. Cremades, A. C. Sterling, C. H. Mandrini, S. Dasso, S. E. Gibson, D. A. Haber, R. W. Komm, G. J. D. Petrie, P. S. McIntosh, B. T. Welsch, and S. P. Plunkett, “The Global Context of Solar Activity During the Whole Heliosphere Interval Campaign,” *Solar Phys.*, 274, pp. 57-86, 2011.

Webb, David F. and Timothy A. Howard, “Coronal Mass Ejections: Observations,” *Living Rev. Solar Phys.*, (http://www.livingreviews.org/lrsp-2012-3), 9, 3, 2012.

Webb, D. F., T. A. Howard, C. D. Fry, T. A. Kuchar, D. Odstrcil, B. V. Jackson, M. M. Bisi, R. A. Harrison, J. S. Morrill, R. A. Howard, and J. C. Johnston, “Study of CME Propagation in the Inner Heliosphere: SMEI and STEREO HI Observations of the January 2007 Events,” *Solar Physics*, 256, pp. 239-267, 2009.

Webb, D. F., C. Möstl, B.V. Jackson, M. M. Bisi, T. A. Howard, T. Mulligan, E.A. Jensen, L. K. Jian, J. A. Davies, C. A. de Koning, Y. Liu, M. Temmer, J. M. Clover, C. J. Farrugia, R. A. Harrison, N. Nitta, D. Odstrcil, S. J. Tappin, and H.-S. Yu, “Heliospheric Imaging of 3-D Density Structures During the Multiple Coronal Mass Ejections of Late July to Early August 2010,” *Solar Phys, TI: Observations & Modeling of the Heliosphere*, 285, pp. 317-348, 2012.

Woods, Thomas N., Rachel Hock, Frank Eparvier, Andrew R. Jones, Phillip C. Chamberlin, James A. Klimchuk, Leonid Didkovsky, Darrell Judge, John Mariska, Harry Warren, Carolus J. Schrijver, David Webb, Scott Bailey, and W. Kent Tobiska, “New Solar Extreme Ultraviolet Irradiance Observations During Flares,” *Astrophys. J.*, 736, 2011.

Ying, Liu, Janet Luhmann, Christian Moestl, Juan Martinez Oliveros, Stuart Bale, Robert P. Lin, Richard A. Harrison, Manuela Temmer, David Webb, and Dusan Odstrcil, “Interactions between Coronal Mass Ejections Viewed in Coordinated Imaging and In Situ Observations,” *Astrophys. J. Lett.*, 746, L15, 2012.

D. Webb also is a coauthor on two other Decadal Survey papers involving a mission to the L5 point: N. Gopalswamy, et al., “Earth-Affecting Solar Causes Observatory (EASCO): A New View from Sun-Earth L5” and A. Vourlidas, et al., “Mission to the Sun-Earth L5 Lagrangian Point: An Optimal Platform for Heliophysics & Space Weather Research.” All these papers can be found at: http://www8.nationalacademies.org/SSBSurvey/publicviewHeliophysics.aspx.

A paper by Barbara Thompson and 24 coauthors including D. Webb, entitled “A Snapshot of the Sun Near Solar Minimum: The Whole Heliosphere Interval,” was published by Solar Physics in the Whole Heliosphere Interval (WHI) Topical Issue vol. 174, nos. 1 and 2. This is an overall review of all the science activities that came out of the WHI Campaign period. The URL of the topical issue is: http://www.springerlink.com/content/u86q31127twx/.

Presentations

Gibson, S. E., et al., “End-to-end observations and modeling of Whole Heliosphere Interval: Origins and impacts of high-speed streams,” Abstract SH21B-01, poster presented by Webb, David, AGU Meeting of the Americas, Foz do Iguassu, Brazil, 8-12 August 2010.

Ginet, Gregory, S. Huston, D. Madden, C. J. Roth, and T. P. O’Brien, “The Trapped Proton Environment in Medium Earth Orbit (MEO),” Presented (by G. P. Ginet) at IEEE Nuclear and Space Radiation Effects Conference (NSREC), Denver, CO, 20 July 2010.

Howard, Timothy A. and David F. Webb, “Utilizing Heliospheric Imagers to Improve Space Weather Forecasting,” IUGG 2011 General Assembly, Melbourne, Australia, Program Book, A121S5, p. 202, 6 July 2011.

Huston, S., “Proton Flux Maps,” Presented at AE/AP-9 Critical Design review, Chantilly, VA, 10 Nov. 2009.

Johnston, J. C., T. A. Kuchar, and David Webb, “SH54D-01: The Role of Short-Term Precursors in a Hybrid CME Forecast,” (Invited talk), p. 557, AGU Fall Meeting Program, 13-17 Dec. 2010.

Johnston, J., T. Kuchar, and David Webb, “Forecasting Geomagnetic Storms: Tracking Hazardous Solar Ejecta with the Next Generation Heliospheric Imaging System,” a poster presented at the SEASONS 2010 conference on Space Weather held in Washington, DC, Nov. 2-4, 2010.

Johnston, J. C., T. A. Kuchar, David Webb, and T. A. Howard, “Space Weather Forecasting Laboratory: Constructing a Hybrid CME Forecast Methodology,” SH42A-02, invited talk by J. Johnston, AGU Meeting of the Americas, Foz do Iguassu, Brazil, 8-12 August 2010.

Lin, Chin S., Delores Knipp, Frank Marcos, Samuel B. Cable, and Eric K. Sutton, “Survey of Thermosphere Joule Heating Locations and Magnetic Disturbance Conditions,” AGU Fall Meeting, 2011

Perry, K. L., “AFWA Rules of Thumb Validation,” AFWA, Omaha, Nebraska, July 2010.

RAL SWx Group, “Space weather mission trade-offs for Heliospheric Imaging,” L5 NGHI workshop, Sunspot, NM, April 21-22, 2011.

Sutton, Eric K., Samuel B. Cable, Frank A. Marcos, and Chin S. Lin, “Improved Basis Functions for Dynamic Calibration of Semi-Empirical Thermospheric Models,” AGU Fall Meeting, 2011.

Webb, D. F., “Comparison of Solar Wind and Transient Data During the Last Two Solar Minima,” Abstract SH14A-03, invited talk, AGU Meeting of the Americas, Foz do Iguassu, Brazil, 8-12 August 2010.

Webb, D. F. and S. E. Gibson, “How Do the Current Solar Wind and CME Data Compare to the Previous Minimum?”, invited talk at the 10th SORCE meeting held in Keystone, CO, May 18-21, 2010.

Webb, David, “STEREO & SMEI Observations Pertinent to LWS MC CDAW,” NASA LWS CDAW, Predictive Science in San Diego, CA, September 21-24, 2010.

Webb, David, “STEREO Events Pertinent to LWS MC CDAW Group,” NASA LWS CDAW, Predictive Science in San Diego, CA, September 21-24, 2010.

Webb, David, presentation of his CME heliospheric imaging results for the ISR Seminar at St. Clements Hall, March 1, 2011.

Webb, David, presentation of SMEI and STEREO HI results for the January 2010 event at the AFRL staff reports meeting at AFRL- Hanscom on April 6, 2011.

Webb, David, presentation of SMEI and STEREO HI results involving space weather at the annual SWFL review meeting at AFRL- Hanscom on Feb. 24, 2011.

Webb, David, presented the NGHI concept at a Town Hall meeting on the Decadal Survey at the Univ. of New Hampshire, Durham, NH held on Nov. 8, 2010.

Webb, David, spoke at a NASA Briefing on NASA Data and New Techniques Yield Detailed Views of Solar Storms held at NASA HQ on 18 August 2011.

Webb, David, “STEREO Space Weather Beacon,” L5 NGHI workshop, Sunspot, NM, April 21-22, 2011.

Webb, David, “The Characteristics of CMEs from Combined STEREO Imaging and In-situ Observations,” Stereo-4/SDO-2/SOHO-25 Workshop, July 25 - 29, 2011, at Christian-Albrechts-Universität, Kiel, Germany. Abstract Book, p. 31, 28 July 2011.

Webb, David, “The Global Context of Solar Activity During the Whole Heliosphere Interval Campaign,” poster at the American Astronomical Soc./Solar Physics Div. meeting held in Miami FL, 23-27 May 2010.

Webb, David, D. Biesecker, N. Gopalswamy, O. C. St. Cyr, J. M. Davila, and, K. Simunac, “Using STEREO-B as an L5 Space Weather Pathfinder Mission,” L5 NGHI workshop, Sunspot, NM, April 21-22, 2011.

Webb, David, M. M. Bisi, C. A. de Koning, R. A. Harrison, T. A. Howard, B. V. Jackson, J. C. Johnston, E. Kilpua, T. Kuchar, C. Moestl, and J. Tappin, “Studying the Characteristics of CMEs Using Combined Imaging and In-situ Data from STEREO, SOHO and other L1 spacecraft, SMEI and SDO,” IUGG 2011 General Assembly, Melbourne, Australia, Program Book, A101S6, p. 144, 3 July 2011.

Webb, David, E. W. Cliver, N. V. Nitta, G. D. Attrill, K. Marubashi, T. A. Howard, J. Tappin, and B. V. Jackson, SH41A-1778 POSTER: “End-to-End Observations and Modeling of the 17-21 January 2010 CME/ICME,” p. 377, AGU Fall Meeting Program, 13-17 Dec. 2010.

Webb, David, J. C. Johnston, T. A. Kuchar, J. Tappin, and T. A. Howard, “SH54D-05: Forecasting Earth Arrivals of CMEs with Heliospheric Imagers,” (Invited talk), p. 557, AGU Fall Meeting Program, 13-17 Dec. 2010.

LIST OF SYMBOLS, ABBREVIATIONS, AND ACRONYMS

1-D	One Dimensional
2-D	Two Dimensional
3-D	Three Dimensional
ACE	Advanced Composition Explorer
ACS	Altitude Control System
AFB	Air Force Base
AFGEOSpace	Air Force GEOSpace Model
AFRL	Air Force Research Laboratory
AFSPC	Air Force Space Command
AFWA	Air Force Weather Agency
AIA	Atmospheric Imaging Assembly
AE-8	Trapped Electron Model – version 8
AE-9	Trapped Electron Model – version 9
AP-8	Trapped Proton Model – version 8
AP-9	Trapped Proton Model – version 9
APEX	Active Plasma Experiment Satellite
AU	Astronomical Unit
BC	Boston College
BRAC	Base Realignment and Closure
CEASE	Compact Environmental Anomaly Sensor
CDAW	Coordinated Data Analysis Workshop
CME	Coronal Mass Ejection
COSMIAC	Configurable Space Microsystems Innovations and Applications Center
CRRES	Coordinated Radiation Release Satellite
DAC	Data Analysis Center
DST	Magnetic Activity Index
DSX	Deployable Structures Experiment
EPAM	Electron, Proton and Alpha Monitor
EUV	Extreme Ultraviolet
EVE	Extreme Ultraviolet Variability Experiment
FITS	Flexible Image Transport
GOES	Geosynchronous Operational Environmental Satellite
GUI	Graphical User Interface
HAF	Hakamada-Akasofu-Fry solar wind model
HEO	High Earth Orbiter
HF	High Frequency
HI(s)	Heliospheric Imager(s)
HI-A	Heliospheric Imager viewing east of the Sun-Earth line
HI-B	Heliospheric Imager viewing west of the Sun-Earth line
ID	IDentification
IP	Interplanetary Propagation
IPS	Imaging Proton Sensor
ISR	Institute for Scientific Research
ISSI	International Society for Scientometrics and Infometrics

KeV	Kiloelectron Volt
Kp	Magnetic Activity Index
LANL	Los Alamos National Laboratory
LASCO	Large Angle and Spectrometric Coronograph
L_m	Planetary Magnetic Field Parameter
MeV	Mega Electron Volt
MIC	Multiple Instrument Chamber
MITLL	Massachusetts Institute of Technology Lincoln Laboratory
Mk	Micro kelvin
MK3	Third Generation Anomaly Sensor
NASA	National Aeronautics and Space Administration
NM	New Mexico
NOAA	National Oceanic and Atmospheric Administration
NRO	National Reconnaissance Office
NRT	Near Real Time
OSX	Operating System Extension
PAD	Polar Auroral Dynamics
PCA	Principal Component Analysis
PI	Principal Investigator
PRF	Point Response Function
RBSP	Radiation Belt Storm Probes
RVB	Battlespace Environment Division of AFRL
S3-3	3-inch Proton Telescope
SDO	Space Dynamics Observatory
SECCHI	Sun-Earth Connection Coronal Heliosphere Investigation
SEP	Solar Energetic Particle
SEPEM	Solar Energetic Particle Environment Modelling
SEPMOD	Solar Energetic Particle Model
SKp	Daily average solar wind speed
SMEI	Solar Mass Ejection Imager
SNRTACS	Space Nuclear Radiation Threat Assessment Code System
SOHO	Solar and Heliospheric Observatory
SPE	Solar Particle Events
SPLP	Second Planar Langmuir Probe
STEREO	Solar Terrestrial Relations Observatory
STOA	Shock Time of Arrival Model
STP	Space Test Program
SWFL	Space Weather Forecast Laboratory
TacSat4	Tactical Satellite 4
TB	Terabyte
T-H	Tappen-Howard Model
TOA	Time of Arrival
TSX 5	Tri-Service-Experiments Mission 5 Satellite
TWINS	Two Wide-angle Imaging Neutral-atom Spectrometers
UCSD	University of California, San Diego
UV	Ultraviolet radiation

V_H	horizontal plasma drift
WHI	Whole Heliospheric Interval
WSA	Wang-Sheeley-Arge
XML	Extensible Markup Language

DISTRIBUTION LIST

DTIC/OCP 8725 John J. Kingman Rd, Suite 0944 Ft Belvoir, VA 22060-6218	1 cy
AFRL/RVIL Kirtland AFB, NM 87117-5776	2 cys
Official Record Copy AFRL/RVBX/Dr. Judy Fennelly	1 cy